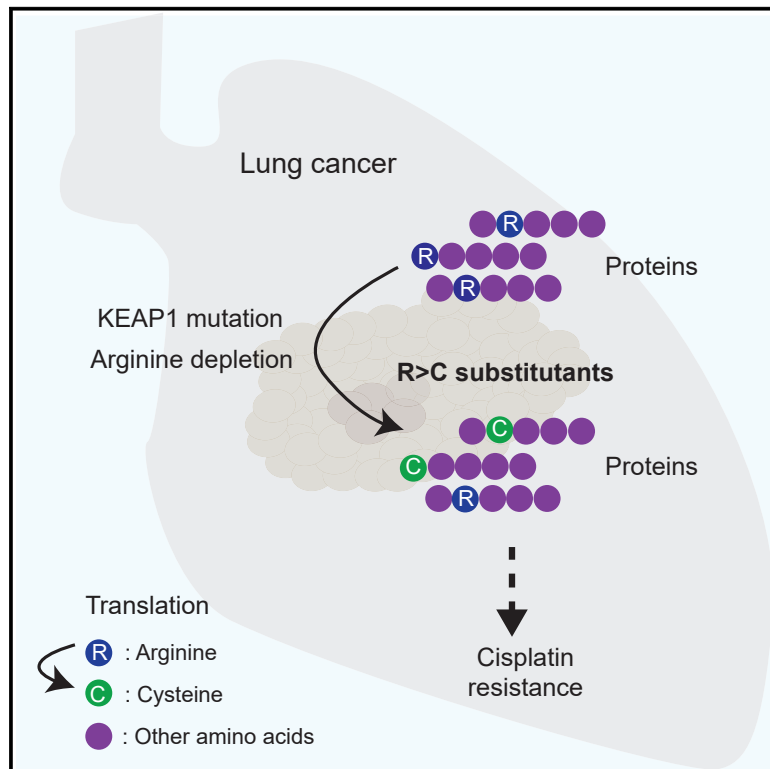# Arginine deprivation enriches lung cancer proteomes with cysteine by inducing arginine-to-cysteine substitutants

Graphical abstract

Authors

Chao Yang, Abhijeet Pataskar, Xiaodong Feng, ..., Celia R. Berkers, Onno B. Bleijerveld, Reuven Agami

Correspondence

a.pataskar@nki.nl (A.P.), r.agami@nki.nl (R.A.)

In brief

Yang, Pataskar, et al. investigated the impact of arginine shortage on aberrant mRNA translation in cancer. They report the enrichment of arginine-to-cysteine substitutants in human lung cancer, link it to a tRNA misalignment mechanism, and connect it to KEAP1 pathway mutations and platinum resistance.

Highlights

- Arginine-to-cysteine (R>C) substitutants are enriched in lung cancers with KEAP1 pathway mutations

- Arginine deprivation induces R>C substitutants

- tRNA misalignment is a proposed mechanism for R>C substitutants in lung cancer

- R>C substitutants may enhance resistance to cisplatin treatment

CellPress

Article

Arginine deprivation enriches lung cancer proteomes with cysteine by inducing arginine-to-cysteine substitutants

Chao Yang,[1,5] Abhijeet Pataskar,[1,5,*] Xiaodong Feng,[1] Jasmine Montenegro Navarro,[1] Inés Paniagua,[1] Jacqueline J.L. Jacobs,[1] Esther A. Zaal,[2] Celia R. Berkers,[2] Onno B. Bleijerveld,[3] and Reuven Agami[1,4,6,*]

[1]Division of Oncogenomics, Oncode Institute, The Netherlands Cancer Institute, Amsterdam, the Netherlands
[2]Division of Cell Biology, Metabolism & Cancer, Department Biomolecular Health Sciences, Faculty of Veterinary Medicine, Utrecht University, Utrecht, the Netherlands
[3]NKI Proteomics Facility, The Netherlands Cancer Institute, Amsterdam, the Netherlands
[4]Erasmus MC, Department of Genetics, Rotterdam University, Rotterdam, the Netherlands
[5]These authors contributed equally
[6]Lead contact
*Correspondence: a.pataskar@nki.nl (A.P.), r.agami@nki.nl (R.A.)
https://doi.org/10.1016/j.molcel.2024.04.012

SUMMARY

Many types of human cancers suppress the expression of argininosuccinate synthase 1 (ASS1), a rate-limiting enzyme for arginine production. Although dependency on exogenous arginine can be harnessed by arginine-deprivation therapies, the impact of ASS1 suppression on the quality of the tumor proteome is unknown. We therefore interrogated proteomes of cancer patients for arginine codon reassignments (substitutants) and surprisingly identified a strong enrichment for cysteine (R>C) in lung tumors specifically. Most R>C events did not coincide with genetically encoded R>C mutations but were likely products of tRNA misalignments. The expression of R>C substitutants was highly associated with oncogenic kelch-like epichlorohydrin (ECH)-associated protein 1 (KEAP1)-pathway mutations and suppressed by intact-KEAP1 in KEAP1-mutated cancer cells. Finally, functional interrogation indicated a key role for R>C substitutants in cell survival to cisplatin, suggesting that regulatory codon reassignments endow cancer cells with more resilience to stress. Thus, we present a mechanism for enriching lung cancer proteomes with cysteines that may affect therapeutic decisions.

INTRODUCTION

Amino acids are not only the basic building blocks of proteins but also are essential metabolites for the production of nucleotides, antioxidants (e.g., glutathione), and energy (e.g., components of the tricarboxylic acid cycle).[1] Although amino acids are important nutrients for tumor progression, they are also essential for immune cell function and efficient anti-tumor activity.[2] These dependencies ignite a competition state between tumors and immune cells within the tumor microenvironment. In particular, T cells, the critical players in anti-tumor immunity, rely heavily on amino acid transportation and metabolism for their activation, differentiation, and function.[3,4] Thus, tumor cells manipulate amino acid metabolism not only for their own proliferation and invasion benefit but also to enable tumor immune evasion.[1,5,6] Noticeable among those pathways is the enhanced catabolism of amino acids by cancer cells to produce metabolites that suppress the immune response at the tumor surrounding.[2] But equally important, tumors accelerate the uptake and usage of amino acids required for immune cell function to void the microenvironment from key amino acids and suppress anti-tumor immunity.[7,8]

Arginine is a prominent example of an amino acid that is a key player in the interaction between cancer cells and anti-tumor immunity. Loss of Solute Carrier Family 7 Member 1 (SLC7A1), a main arginine transporter, impairs arginine uptake and T cell proliferation.[9] Furthermore, arginine deprivation reduces T cell proliferation and cytokine production,[9,10] while arginine supplementation promotes the generation of central memory-like T cells with high survival capacity.[11] Thus, T cell function and, hence, anti-tumor activity are enhanced by arginine.

Given this compelling anti-tumor impact of arginine, it is not surprising that intracellular arginine production is suppressed in many tumors—mainly by repressing the expression of argininosuccinate synthase 1 (ASS1), a rate-limiting arginine synthetase enzyme.[12–14] This boosts *de novo* nucleotide production,[15] but also promotes arginine auxotrophy that imposes an arginine-restrictive tumor microenvironment with reduced anti-tumor activity.[11,16] In addition to suppressing arginine production, arginine catabolism contributes to cancer immune evasion too. Increased arginase 1 (ARG1) secretion in tumors and M2 macrophages can further limit arginine levels in the tumor microenvironment.[17] Furthermore,
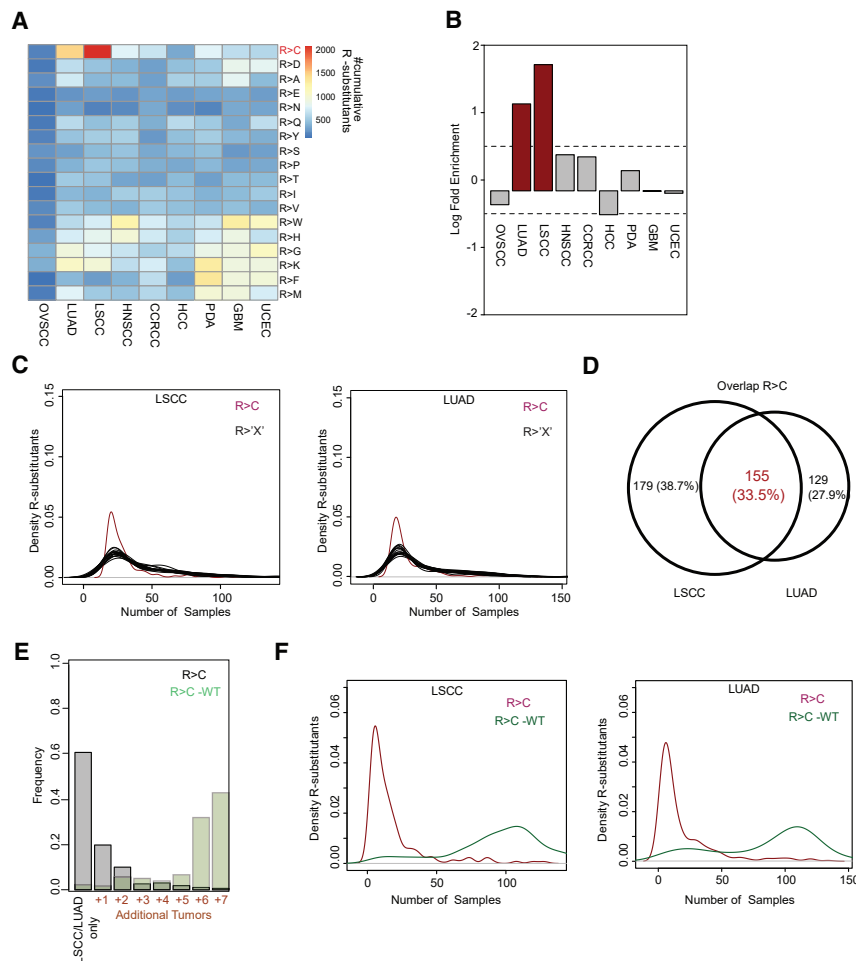
Figure 1. Strong and specific enrichment of arginine-to-cysteine (R>C) substitutions in lung cancer

(A) Heatmap depicting the cumulative number of arginine substitutions detected in proteomics datasets of nine human cancer types sourced from CPTAC.[21]

(B) Bar plot depicting log-fold enrichment in numbers of R>C substitutions in nine human cancer tissues. Vertical lines mark absolute levels of 1.5-fold differences.

(C) Left: density plot depicting the number of samples of LSCC datasets ($n = 207$) where a particular arginine substitution is detected. R>C substitutions are depicted as a dark red line, while all other substitutions are depicted as black lines. The x axis denotes the number of samples, while the y axis denotes density. Right: the same analysis as left but for LUAD ($n = 217$) datasets.

(D) A Venn diagram showing the overlap of the R>C substitutions found in the LSCC and LUAD datasets.

(E) Bar plot depicting the frequency of R>C substitutions (R>C, gray) or the corresponding wild-type (WT) peptides associated with the detected R>C substitutions (R>C-WT, green) in LSCC and LUAD tumors only (first bar) or in every additional tumor across the 9 analyzed human cancer types.

(F) As in (C) but for R>C substitutions (R>C, dark red) and WT peptides associated with R>C substitution peptides (R>C-WT, dark green). The LSCC and LUAD datasets are presented on the right and left, respectively.

arginine catabolism produces nitric oxide, which inhibits anti-tumor T cell responses.[18]

Amino acid shortages can impact mRNA translation in a number of ways. Primarily, amino acid levels are sensed by proteins that regulate global rates of mRNA translation, such as the target of rapamycin complex 1 (TORC1) signaling pathway, a master regulator of cell growth and metabolism.[19] However, amino acid shortages can also impact the quality by which proteins are produced. In human cancer, this is exemplified by the essential amino acid tryptophan. Tryptophan is catalyzed by indoleamine-2,3-dioxygenase 1 (IDO1) in response to interferon-gamma secreted by activated T cells. Although tryptophan levels become limiting, mRNA translation across the tryptophan codons can proceed in cancer cells via ribosomal frameshifting and codon usage reassignment (substitutants) mechanisms.[20–25] Here, we interrogated the consequences of establishing an effective anti-tumor immunity through arginine shortage to protein production in cancer.

RESULTS

Specific strong enrichment of arginine-to-cysteine (R>C) substitutions in lung cancer

To investigate the potential consequences of suppression of arginine production to mRNA translation in human tumors, we inspected the Clinical Proteomic Tumor Analysis Consortium (CPTAC [https://proteomic.datacommons.cancer.gov/pdc/][21]) dataset for the appearance of substitution events of arginine codons to any other amino acid (R>X) from expressed proteins. The most pronounced event we found was an enrichment of R>C substitutions in lung cancer patients (i.e., lung squamous cell carcinoma (LSCC) and lung adenocarcinoma (LUAD), Figures 1A, 1B, and S1A). A weaker and non-tissue-specific signal was also detected for a few other arginine substitutions (e.g., lysine [R>K], histidine [R>H], and tryptophan [R>W]). Additionally, R>C demonstrated a higher sample-specificity enrichment compared with all other R>X, suggesting that R>C substitutions are highly regulated by biological events in lung cancer (Figure 1C). No specific enrichment pattern of other arginine substitutions was observed in all other investigated tumor types (Figure S1B; Table S1). To identify arginine substitutions, we used Philosopher, a "spectrum-centric" approach,[22] which we validated with "a peptide-centric" approach using a universal targeted peptide search engine (PEPQUERY2).[23] Here, too, we observed lung cancer-specific enrichment of R>C peptides even after stringent filtering (Figures S1C and S1D). Thus, R>C substitutions are less consistently expressed across tissues, suggesting a biological relevance in lung cancer.

A

B
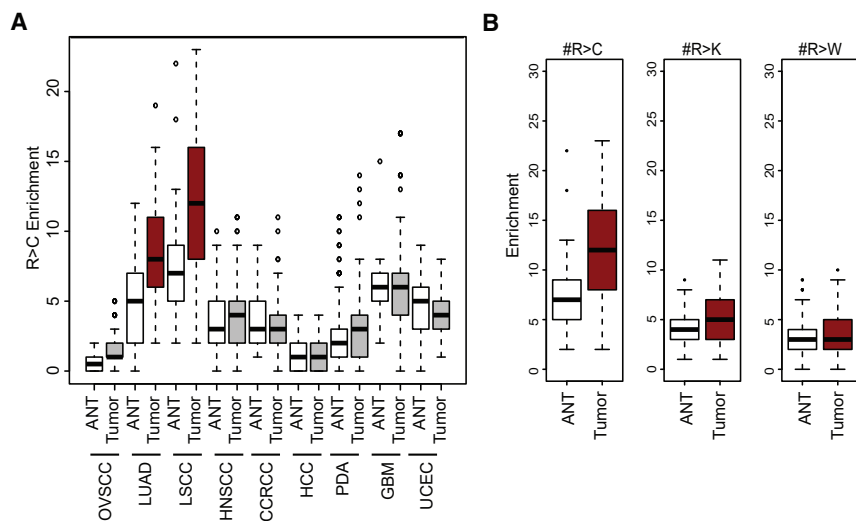
Figure 2. Tumor enrichment of R>C substitutions in lung cancer

(A) Box plot depicting the enrichment of R>C substitutants in adjacent normal tissues (ANT) and tumors in nine human cancer types. LSCC and LUAD tumors are plotted in dark red, other tumors are plotted in gray, and ANT is plotted in white.

(B) Box plot depicting R>C enrichment (left), R>K enrichment (middle), and R>W enrichment (right) in ANT and tumors of the LSCC dataset.

An intriguingly significantly large portion of R>C peptides was shared between the two LSCC and LUAD lung cancer types (33.5%, 155 out of 463 peptides, $p < 0.001$, Figure 1D), suggesting a selective production process. Supporting this idea, we found that a large proportion (0.6, 305 peptides) of the LSCC and LUAD-expressed R>C peptides are not detected in any other tissue type in our dataset (Figure 1E). The R>C peptides that were found only in LSCC and LUAD are further characterized by a low number of unique spectral assignment (peptide-spectral matches) (Figure S1E, $p = 2.2e^{-16}$), suggesting that they are distinctive and specific to these tissues. This unique expression pattern of R>C peptides in LSCC and LUAD was not a result of their host gene expression, as determined by the analysis of the corresponding wild-type (R>C-WT) peptides containing arginine residues (Figures 1E and S1F). In this analysis, a fraction of the R>C-WT peptides could be tested due to the additional trypsin cleavage of arginine generating, on some occasions, too short peptides to be analyzed by mass spectrometry (Figures S1G and S1H). Nevertheless, in contrast to R>C peptides, the pattern of the detectable R>C-WT peptides was observed to be normally distributed (Figures 1E and 1F), pinpointing once more the unique biological relevance of R>C peptides in lung cancer. Altogether, large-scale proteomics analyses of human cancer suggest R>C substitution events are uniquely and largely commonly expressed in the lung-related cancer types LSCC and LUAD.

**Tumor-enriched expression of R>C substitutions in lung cancer**

Intrigued by the tissue specificity of R>C substitutions, we further investigated their tumor expression pattern in LSCC and LUAD. To correct the distribution bias, we filtered out peptides that were seen in more than 25% of samples across all substitution classes (Figure 1C). Figure 2A shows that in both lung tissues, with a stronger signal in LSCC, tumors were significantly enriched in R>C peptides compared with their adjacent normal tissues (ANT) ($p < 2.2e^{-16}$). In comparison, no significant tumor enrichment

was observed for control R>K and R>W peptides in LSCC and LUAD (Figures 2B and S2), and no tumor enrichment was observed for R>C peptides in other tissues beyond LSCC and LUAD (Figure 2A). These results indicate that in lung cancer, tumors are the main source of proteins with R>C substitutions.

Most R>C events are substitutants caused by tRNA-cysteine misalignment

Given our findings, we inquired about the causal events that produce R>C proteins in lung cancer. Increased mutagenesis is a hallmark of cancer, with only a few "driver" oncogenic and tumor-suppressive mutations.[24] Previous analysis of all nonsynonymous single nucleotide substitutions (~2,000 proteins, >18,000 cancer samples) revealed cysteine gain at the expense of arginine loss (R>C) as the most frequent genetic event.[25] Furthermore, it was recently observed that arginine limitation could drive codon-specific DNA evolution, possibly leading to R>C substitutions.[26] Thus, we initially suspected that the R>C signal in CPTAC lung cancer proteomes could originate from somatic mutations in these tumors, though the relatively large overlap between the R>C peptides in LSCC and LUAD (Figure 1E) does not support this notion. Indeed, when we examined the overlap between the identified genetic R>C somatic mutations and R>C peptides from the same CPTAC cohorts of LSCC and LUAD tumors, no overlap was observed (Figure 3A). We did not detect any R>C genetic mutations partly because of mass spectrometry limitations and partly due to our peptide library strategy—replacing every arginine residue with cysteine, resulting in only 32 predicted mutated peptides. When codon-specific arginine substitution libraries were examined (now containing 133 predicted mutated peptides) in the LSCC proteomic dataset, 4,900 R>C peptides were detected, of which only three emerged from genetic mutations (Tumor Protein P53 [TP53]^{R273C}, Laminin Subunit Alpha 2 [LAMA2]^{R1366C}, and Histone Cluster 1 H4 Family Member E [H4C5]^{R56C}; Figure S3A; Table S2). Altogether, these results indicate that the vast majority of the R>C peptides detected in LSCC and LUAD cancer proteomes are the result of regulated codon reassignments (substitutants) that are generated by aberrant mRNA translation.

Non-genetic R>C substitutants were not detected in previous attempts to identify amino acid substitutions in bacteria, yeast, plants, or mammals.[28,29] To validate R>C events and obtain
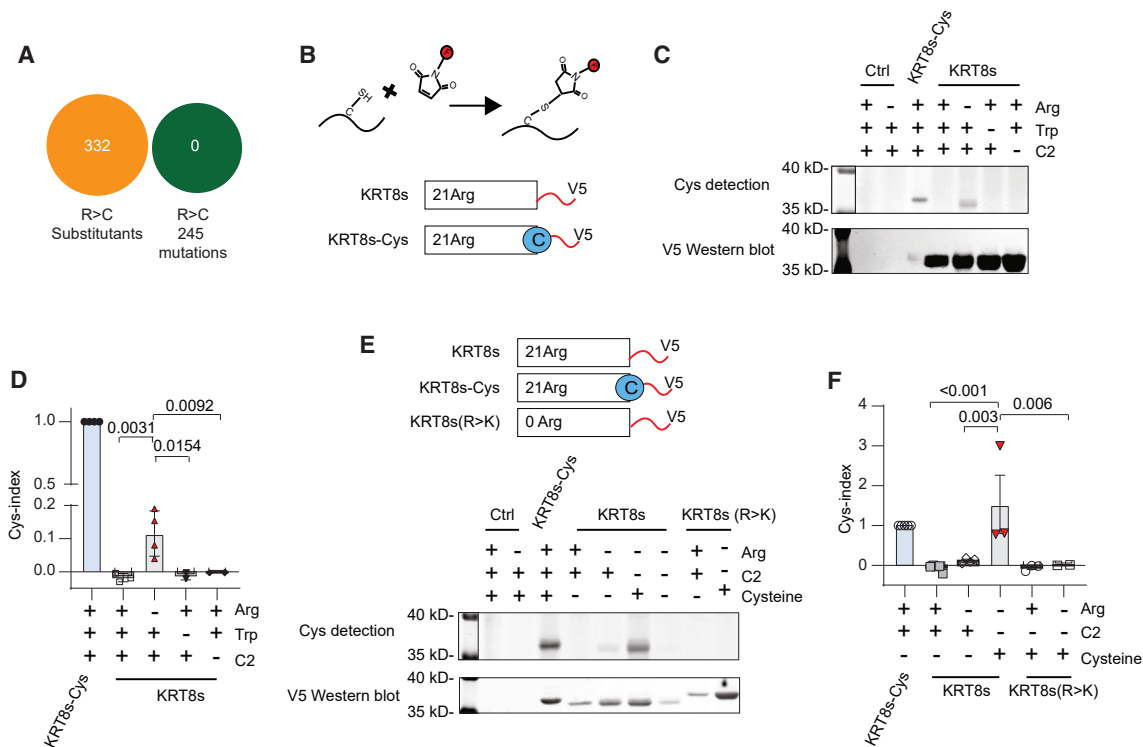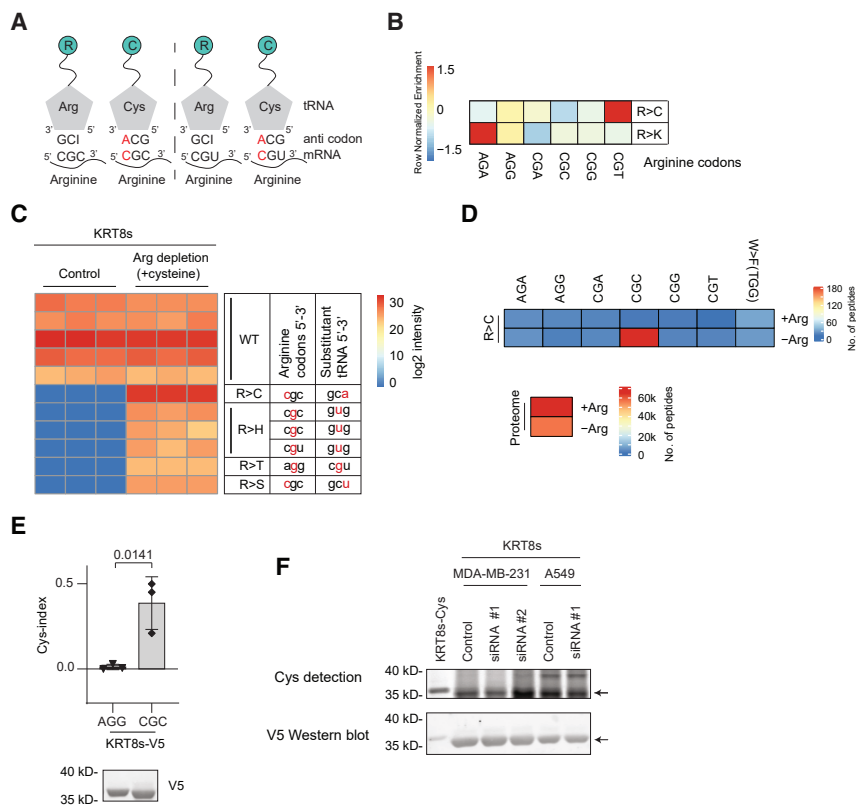
Figure 3. R>C substitutions are substitutants induced by arginine depletion

(A) A Venn diagram depicting the lack of overlap between the detected R>C substitutions in LSCC proteomes and the genetic mutations identified that lead to R>C mutants in LSCC genomes. The genetic mutations were sourced from the original analyzed study.[27]

(B) A scheme illustrating the biochemical assay we developed for detecting protein-incorporated cysteines.

(C) Protein-incorporated cysteine assay was performed on cell populations expressing either KRT8s-V5 or KRT8s-Cys-V5. Cells were deprived of either arginine (Arg), tryptophan (Trp), and cystine (C2) for 3 days, as indicated. Anti-V5 immunoblot assessed reporter protein expression.

(D) Quantification of protein-incorporated cysteine using Cys-index. The bar plot represents at least 3 independent experiments, and the p values were calculated by one-way ANOVA with Sidak's multiple comparisons test.

(E) Upper: a scheme depicting the reporter vectors used in this experiment. Lower: a representative protein-incorporated cysteine assay.

(F) Cys-index of protein-incorporated cysteine experiments as presented in (E). The bar plot represents 2–6 independent experiments, and the p values were calculated by one-way ANOVA with Sidak's multiple comparisons test.

further mechanistic insight into this process, we designed a biochemical reporter assay. We used a fluorescently labeled maleimide reagent to detect cysteines incorporated into proteins and constructed a reporter vector containing a V5-tagged fragment of keratin 8 amino acids 205–483 (KRT8s-V5: UniProt: P05787) that contains 21 arginine residues but no cysteine (Figure 3B). As a positive control for this assay, we constructed a KRT8s-V5 reporter vector containing a short-extended carboxyl terminus with one cysteine residue (KRT8s-Cys-V5, Figure 3B). For these assays, we employed MDA-MB-231 cells, which are auxotrophic to arginine due to the low expression level of ASS1 (Figure S3B[30]). In line with the auxotrophic behavior of these cells, arginine depletion induced the inhibitory phosphorylation of the translational elongation factor eIF2A (Figure S3C). We, therefore, stably transduced these cells with the described KRT8s-V5 reporter constructs and then deprived them of arginine. As controls, we depleted the cells from either tryptophan or cystine (C2), the oxidized dimer form of cysteine that is typically added to culture media to supplement cells with cysteine. We generated whole-cell extracts and immunoprecipitated and

eluted KRT8s-V5 proteins to examine protein-incorporated cysteine. As expected, a clear cysteine signal appeared in V5-eluates from cells expressing KRT8s-Cys-V5, while no cysteine was detected in control non-transduced cells, even when arginine was depleted (Figure 3C). Interestingly, in cells expressing KRT8s-V5, a clear signal was observed only in cells deprived of arginine (Figure 3C). Cells that were treated with a control medium or media depleted from either tryptophan or C2 did not show any detectable cysteine in the KRT8s-V5 reporter protein (Figure 3C). Immunoblot analysis of the same eluates validated the presence of KRT8s-V5 protein in the eluates (Figure 3C). To normalize reporter-incorporated cysteine and compare outcomes across various experiments and conditions, we used KRT8s-Cys-V5 as an internal standard control for each experiment (analysis named Cys-index). This quantification estimated cysteine incorporation to KRT8s-V5 following arginine depletion to be ~0.1 Cys-index in four biological replicates (Figure 3D, p = 0.0031). Similar results were obtained using the lung cancer cell line A549 (Figures S3D and S3E, p = 0.001), which is in line with the identification of R>C in lung cancer proteomes (Figure 1).

Figure 4. R>C substitutants are produced by tRNA misalignments

(A) A scheme illustrating the potential tRNA misalignment events leading to R>C substitutants. Inosine modification of tRNA-Arg can recognize both CGC and CGT codons. Human cells express only one type of tRNA-Cys (anticodon 5′-GCA-3′). The mismatch positions at both CGC and CGU codons are marked with red letters.

(B) Heatmap depicting row-scaled enrichment of the percentile differences in the codon numbers over expected distribution. LSCC cancer proteomes were used for this analysis.

(C) V5-IP/MS analysis of MDA-MB-231 cells containing a doxycycline-inducible KRT8s-V5 reporter vector. Heatmap indicates the intensities of peptides assigned to the reporter protein (WT) or R>X substitutants emerging following arginine depletion. R, arginine; C, cysteine; H, histidine; T threonine; and S, serine. The corresponding arginine-reporter codons of the detected substitutants are annotated.

(D) Heatmap depicting the number of R>C substitutants detected specifically in MDA-MB-231 cells cultured with or without arginine (+Arg and −Arg, respectively) in the presence of cysteine. Only the peptides detected in three biological replicates ($n = 3$) of every condition were selected.

(E) Cys-Index (upper panel) and immunoblot analyses (lower panel) of MDA-MB-231 cells expressing KRT8s-V5 reporters, where all their arginine codons were either mutated to AGG or CGC. Cells were treated with an arginine depletion medium supplemented with cysteine instead of C2. The bar plot represents 3 independent biological experiments, and the p value was calculated by one-way ANOVA with Sidak's multiple comparisons test.

(F) A protein-incorporated cysteine assay was performed on cells transfected with either control or siRNAs targeting RARS1. V5 immunoblot analysis was used to evaluate the levels of reporter proteins in the eluates. Immunoblot analysis validated the efficiency of RARS knockdowns (Figure S4G).

Next, we investigated arginine-deprivation-mediated cysteine incorporation in cells cultured with cysteine instead of C2. We found no significant difference in the total tRNA^{Arg}(CCG) in cells treated with arginine depletion supplemented with C2 or cysteine (Figure S3F). However, replacing C2 with cysteine augmented cysteine tRNA charging in arginine depletion conditions (Figure S3G) and, importantly, significantly increased Cys-index ~10-fold (to ~1, Figures 3E and 3F, $p = 0.003$). As a control for this experiment, we used KRT8s(R>K)-V5, a KRT8s reporter version where all of its 21 arginine codons were mutated to lysine residues. Although highly expressed (Figure S3H), no detectable cysteine incorporation to this protein was observed following arginine depletion, even when cells were cultured with cysteine in the medium (Figures 3E and 3F, $p = 0.006$).

R>C substitutants can theoretically be induced by tRNA-cysteine (tRNA-Cys-GCA) misalignment to two of the six arginine codons (CGC and CGU nucleotides) when arginine levels are short (Figure 4A). Indeed, the identified R>C peptides in LUAD and LSCC, as well as in the whole CPTAC cohort, showed an enrichment of CGU arginine codons and highlighted tRNA misalignment as the causal mechanism (Figures 4B, S4A, and S4B). By contrast, R>K substitutants, which were consistently present in the CPTAC dataset search (Figures 1B and S1C; Table S3), showed a codon bias to AGA and AGG, which can

be explained by misalignment of tRNA-Lys-UUU and tRNA-Lys-CUU to AGA and AGG codons of arginine, as was suggested before[28] (Figures 4B, S4A, and S4B). To investigate codon bias events in R>C, we used immunoprecipitation-mass spectrometry (IP/MS) analysis in cells containing an inducible KRT8s-V5 reporter vector and cultured with cysteine. This experiment validated the efficient induction of R>C substitutant reporter peptides following arginine depletion in the presence of cysteine (Figures 4C, S4C, and S4D). Furthermore, this experiment also identified additional substitutant events, including R>H, R>T, and R>S, albeit with much lesser intensities (Figure 4C, <0.03-fold), indicating R>C as the prime substitutant event under these culture conditions. R>C incidents were also confirmed in two cell lines carrying a none-inducible KRT8s-V5 reporter vector, an experiment that identified additional arginine substitutant events (e.g., R>K, R>Q, and R>W, Figures S4E and S4F). In these KRT8s-V5 IP/MS validation experiments, codon usage bias was clearly observed. Although R>C showed restricted incorporation to CGC and CGU arginine codons, other events showed other preferences (e.g., R>H CGC and CGU, R>T AGG, R>S CGC, R>K to AGG, R>Q, and R>W to CGG; Figures S4E and S4F). Most of the detected substitutant events, though not all (e.g., R>N and R>L), could be explained by tRNA misalignments. In these *in vitro* experiments, R>C substitutants were enriched

for CGC codons, while in patient tumors, R>C peptides were enriched with CGU codons (Figure 4B). This difference may potentially be explained by the acute depletion of arginine *in vitro*, which does not precisely mimic the intricate metabolic complexity of a tumor.

We further complemented these reporter experiments with a multi-fractionated whole proteome analysis of MDA-MB-231 cells supplemented with cysteine and either deprived or not of arginine. Searching for codon-resolved R>C substitutant peptides, only CGC codons showed strong enrichment in arginine-depleted conditions (Figure 4D; Table S4). As a control, the previously identified W>F substitutants[31] showed no enrichment or specificity (Figure 4D). These results validate both R>C enrichment and codon-specificity.

Next, we assessed R>C codon bias events biochemically. We generated cells stably expressing KRT8s-V5 with all arginine codons modified to either AGG or CGC. In line with the MS results, efficient protein incorporation of cysteine was observed only when CGC codons were used (Figure 4E). Immunoblot analysis confirmed similar levels of KRT8s-V5 of both codon types in the eluates (Figure 4E). To further exclude mis-acetylation of arginine-tRNAs as the underlying mechanism, we knocked down arginyl-tRNA synthetase (RARS) using two small interfering RNA (siRNA) reagents. Although efficient knockdowns were achieved, R>C substitutant levels were generally not reduced following arginine deprivation in the presence of cysteine (Figures 4F and S4G). Thus, arginine shortage stimulates efficient expression of R>C substitutants in the presence of cysteine, with tRNA misalignment as the key mechanism.

R>C substitutants and the ferroptosis pathway

We next inquired about the underlying mechanism that induces R>C substitutants in lung cancer. A major causal candidate is ASS1, whose suppression in tumors limits arginine availability.[12–14] Although ASS1 expression level was reduced in LSCC and LUAD tumors compared with ANT, it was also reduced in many other tumors that did not show a significant R>C signal above background (Figure 5A, e.g., kidney, liver, brain, head and neck, and uterine cancers). This suggests that mechanisms beyond ASS1-mediated suppression of arginine production are needed to explain the presence of R>C substitutants in lung cancer specifically. To identify such mechanisms unbiasedly, we correlated the quantity of R>C peptides with protein expression. Ontology-enrichment analysis of the strongest positively correlating proteins (Figure 5B, R2 correlation coefficient > 0.25, Table S5) indicated positive association with categories related to response to increased oxygen levels, iron metabolism, and the ferroptosis pathway—an iron-dependent form of non-apoptotic cell death (Figures 5C and 5D[32]). Further analysis using a gene signature of ferroptosis genes as well as the entire pathway strengthened this correlation (Figure 5E, $p = 9 \times 10^{-5}$).

In LSCC, frequent KEAP1 (kelch-like ECH-associated protein 1), CUL3 (Cullin 3), and NRF2 (also named NFE2L2 nuclear factor erythroid-derived 2-like 2) mutations (found in approximately 30% of patients[33]) activate a ferroptosis protective response. Under normal conditions, KEAP1 and CUL3 direct an E3 ubiquitin ligase to ubiquitinylate and induce the proteasomal degradation of NRF2, a transcription factor member of the basic leucine

zipper (bZIP) family (Figure 5F, Stockwell et al.[32]). Following ferroptosis stress, NRF2 is stabilized and initiates the transcriptional activation program of genes containing antioxidant response elements in their promotors.[34] We, therefore, explored a gene expression correlation analysis of three direct and prominent proteins that are gene targets of NRF2 and are connected to iron/metal metabolism and protection from ferroptosis (HMOX1, FTH1, and FTL, Dodson et al.[35]). This analysis revealed a positive, strong correlation between these ferroptosis-protecting genes and R>C peptide expression in LSCC tumors (Figure 5G, $p < 0.05$). As controls, actin B (ACTB) and IDO1 proteins did not significantly correlate with R>C peptide expression in LSCC tumors (Figure 5G). To strengthen this potential causal link between the KEAP1 pathway and R>C substitutant expression, we examined R>C peptide levels in mutated KEAP1, CUL3, and NRF2 LSCC tumors (group named KCN, no. of tumors, $n = 31/108$). As a control, we used a similar group size of LSCC tumors containing mutations in phosphatidylinositol-4.5-biphosphate 3-kinase catalytic subunit alpha (PIK3CA) and phosphatase and tensin homolog (PTEN) (group named PP, no. of tumors, $n = 29/108$). As predicted, an enrichment of R>C peptides was only observed in the KCN group of tumors (Figure 5H, $p = 0.09$). As an additional control, we examined R>W peptides, which showed no enrichment in any of the groups (Figure 5H). Thus, LSCC tumors with mutations in genes linked to ferroptosis are the main source of R>C substitutants. We also attempted to explore gene-expression correlation in LUAD tumors but instead found a correlation to the nuclear factor kappa B subunit 1 (NFKB1) signaling pathway, which is known to regulate ferroptosis (Figures S5A and S5B[36]). However, since the signal in LUAD is weaker than LSCC (Figure 1B), we restrict our findings to LSCC only.

Interestingly, the ferroptosis pathway is tightly connected to cysteine metabolism. Constitutive activation of NRF2 by KEAP1-pathway mutations in lung cancer has been reported to induce SLC7A11, a glutamate/C2 antiporter.[37–39] High C2 uptake stimulates cysteine-mediated biosynthesis of the antioxidant GSH (reduced glutathione, glutamyl-cysteinyl-glycine) to inhibit ferroptosis.[37,40] Indeed, Kang et al. recently compared cysteine metabolites in Keap1$^{R554Q/R554Q}$ (R554Q) homozygous mouse embryonic fibroblasts (MEFs) with WT MEFs and annotated the accumulation of intracellular cysteine and its downstream GSH promoted by enhanced NRF2 activity.[41] These observations, together with our finding that supplementing cells with cysteine instead of C2 markedly enhances R>C substitutant levels in arginine-deprived cells, potentially provide an explanation for the association we observed between R>C substitutants and KEAP1-pathway-mediated ferroptosis in lung cancer. To test this connection experimentally, we introduced our cysteine-less KRT8s-V5 reporter vector to A549 lung cancer cells (containing a homozygous G333C inactivation mutation in KEAP1) and ectopically expressed KEAP1-WT in these cells. Proteomics and immunoblot analyses confirmed the expression of KEAP1-WT (Figures 5I, S5C, and S5D). Further inspection of the proteomics also confirmed the downregulation of prime NRF2 targets (FTL, HMOX, and FTH1) and validated the restoration of the cellular response to oxidative stress in KEAP1-WT-expressing A549 cells (Figures 5I and S5E). We therefore cultured
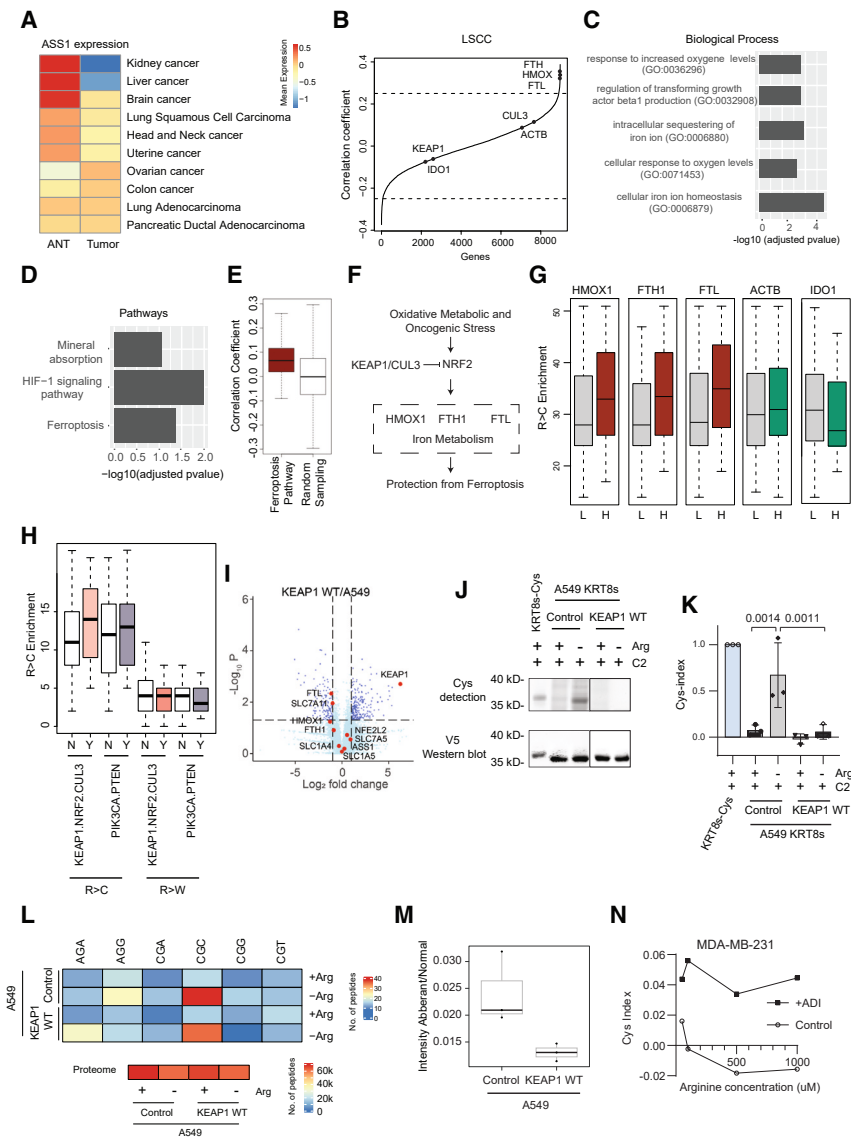
Figure 5. R>C substitutants in LSCC tumors are linked to ferroptosis protection and KEAP1 pathway mutations

(A) Heatmap depicting average expression of ASS1 protein in adjacent normal tissue (ANT) and tumors across multiple cancer types.

(B) Gene rank association plot depicting the correlation coefficients of protein expression levels with the number of R>C substitutants in the LSCC dataset. KEAP1 pathway regulatory genes, target genes, and control genes are highlighted. Vertical lines indicate an absolute cutoff used as 0.25.

(C) A bar plot depicting the $\log_{10}$ adjusted p value of biological processes enriched for genes with a correlation coefficient >0.25 (from B). Ontology analysis was performed by EnrichR.

(D) Same analysis as in (C) but for biological pathways.

(E) Boxplot depicting the correlation coefficients of all ferroptosis genes ($n = 40$) protein expression with R>C enrichment in LSCC tumors.

(F) Oxidative, metabolic, and oncogenic stresses activate NRF2, a transcription factor that controls iron metabolism genes (primarily Ferritin Light Chain [FTL], Ferritin Heavy Chain 1 [FTH1], and Heme Oxygenase 1 [HMOX1]) that induces protection from ferroptosis. KEAP1 and Cul3 genes form an E3 ligase complex restricting NRF2 levels and activity. Frequent mutations in KEAP1, Cul1, and NRF2 in lung cancer induce protection from ferroptosis.

(G) Box plot depicting enrichment analysis of R>C substitutants with the expression of the hallmark ferroptosis genes—HMOX1, FTL, and FTH1. ACTB and IDO1 were used as controls. L denotes tumor samples with lower (<0) gene expression, while H denotes samples where higher (>0) gene expression in LSCC tumors.

(H) Box plot depicts enrichment analysis of R>C or control R>W substitutants with mutations in either KEAP1, NRF2, and CUL3. Samples with PIK3CA and PTEN mutations were used as controls. "N" and "Y" mark the absence and presence of mutations, respectively.

(I) Protein expression analysis of A549-KEAP1-WT vs. A549 control cells.

(J) A representative protein-incorporated cysteine assay was performed with A549 control and KEAP1-WT overexpression cells.

(K) Cys-Index analysis of (J).

(L) Heat map depicting the number of R>C substitutants detected specifically in A549 and A549-KEAP1-WT cells cultured with or without arginine (Arg) in the presence of cysteine. Only the peptides detected in three biological replicates ($n = 3$) of every condition were selected. For reference, a heatmap of the total number of peptides detected in the normal proteome is plotted.

(M) A bar plot depicting the relative intensity of R>C substitutants to normal proteome in A549 and A549-KEAP1 WT cells.

(N) Cys-index analysis of A549 cells incubated with recombinant ADI protein at the indicated concentrations. Corresponding KEAP1 immunoblot is presented in Figure S5C. The bar plot represents 3–4 independent experiments, and the p values were calculated by one-way ANOVA with Sidak's multiple comparisons test.

the cells with C2 and then subjected them to arginine deprivation and examined the efficiency of R>C incorporation into our reporter by V5-IP followed by cysteine incorporation-into-protein assay (Figure 3B). Figures 5J and 5K show a very effective incorporation of cysteine into our cysteine-less-encoded reporter vector in parental A549 cells (Cys-index ~0.5), which was suppressed by the ectopic expression of KEAP1-WT ($p = 0.0011$). To validate this result, we used proteomics analysis and screened every arginine codon for R>C substitutants. Consistent

with our results above (Figure 4D), we observed a significant enrichment of R>C peptides only in CGC codons following arginine depletion (Figure 5L; Table S6). Importantly, in line with the chemical assays (Figures 5J and 5K), both the number of peptides and their relative intensities were significantly lower in KEAP1-WT-expressing cells compared with their parental A549 counterparts (Figures 5L and 5M). Altogether, our findings suggest that R>C substitutants in lung cancer patients are associated with the combined effect of arginine shortage and

cysteine accumulation due to the activation of a ferroptosis protective mechanism by oncogenic mutations in the KEAP1-CUL3-NRF2 pathway.

Arginine-deprivation cancer therapy and R>C substitutants

ASS1-deficient lung cancers are being exploited for therapies using ADI, an arginine deaminase that catabolizes arginine to citrulline and urea.[42–48] We, therefore, examined whether ADI treatment, similar to arginine depletion, provokes R>C substitutants. To test this, we incubated A549-KRT8s-V5 cells with increasing concentrations of arginine in the presence or absence of 1 μg/mL recombinant ADI protein. Cell populations were harvested and subjected to V5-IP followed by cysteine incorporation assays to determine Cys-index. Figure 5N shows that without ADI, supplementation of 100 μM or more of arginine was sufficient to completely block cysteine incorporation into the cysteine-less reporter vector. By contrast, in the presence of ADI, R>C events were still observed even if cells were cultures with up to 1,000 μM arginine. Similar results were obtained with MDA-MB-231 cells, albeit up to 500 μM arginine (Figure S5F). Thus, ADI treatment provokes the expression of R>C substitutants.

R>C substitutants enhance cancer cell survival to chemotherapy

The results above proposed a mechanism underlying the expression of proteins with R>C substitutants in lung tumors. However, in light of the key role of cysteines in scavenging reactive oxygen, it is not inconceivable to hypothesize that tumors may benefit from the appearance of R>C substitutants in their proteome. It has been established that structural cysteines that do not take part in the catalytic functions of proteins can still be important for reactive oxygen scavenging (e.g., Das and Das[49] and Carroll et al.[50]). Moreover, although free cysteine molecules have a very short half-life of ~30 min before being oxidized to C2,[51] incorporated cysteine in proteins may provide longer-term protection. To test whether R>C substitutants can be beneficial for tumors, we first utilized the information that cysteine supplementation accelerates (by ~10-fold) the generation of R>C substitutants relative to C2, and performed growth-competition assays comparing cell behavior in these two culture conditions (Figure 6A). We marked MDA-MB-231 cancer cells with either green or red fluorescence, then pretreated these cell populations with arginine depletion media supplemented with either cysteine or C2 for 3 days. Notably, metabolomic analysis of the cells at this point (3 days) validated arginine depletion and indicated an equilibrium between C2 and cysteine, with moderately more cysteine and C2 in the C2-treated condition (Figure S6A). We explain the increase in R>C by cysteine by higher tRNA charging (Figure S3G) at earlier time points following cysteine addition. Moreover, no difference was observed in the levels of glutathione (GSH and GSSH) in arginine-depleted cells supplemented with either C2 or cysteine (Figure S6A). We then washed and mixed the cells, and following a recovery period of 1 h in normal arginine and C2-containing medium, the cultures were subjected to either mock or cisplatin treatment (Figure 6A). We used cisplatin, as platinum treatment is a first-line chemotherapy treatment for lung cancer and was reported to induce ferroptosis by inhibiting GPX4, glutathione

peroxidase 4.[52] Moreover, KEAP1 pathway mutations were linked to increased resistance to platinum treatment in lung cancer.[53–55] Figure 6B shows that after 21 days of expansion, cells pretreated with arginine depletion plus cysteine had a markedly better survival to cisplatin treatment than C2 ($p < 0.0006$). Here, we calculated the difference from the time zero to normalize with the starting ratios, ranging from 40% to 60%. This survival effect was despite the similar DNA damage levels caused by cisplatin, as measured by histone 2A.X variant γ (H2AX) nuclear intensity staining, and the similar levels of ferroptosis, as measured by 2',7'-dichlorofluorescein deacetate (DCFDA)-cellular reactive oxygen species (ROS) assay (Figures S6B–S6E). We also repeated the treatment A549, a lung cancer cell line with a homozygous KEAP1 G333C mutation. Here, too, pretreatment of arginine depletion plus cysteine provided a survival advantage to cisplatin treatment over arginine depletion plus C2 (Figure 6C, $p < 0.003$). This survival advantage vanished when we overexpressed KEAP1-WT (Figure 6C, $p = 0.44$). Metabolomic analysis showed a similar profile as was observed in MDA-MB-231 (Figure S6A). Again, no significant differences were observed in the amount of DNA damage caused by cis-platin as measured by γH2AX nuclear intensity levels (Figure S6C). This result is in line with the observed KEAP1-WT-mediated suppression of R>C substitutant level (Figures 5J and 5K).

We complemented the cell competition results with cell survival assays. We first pretreated MDA-MB-231 cells with media depleted for either arginine or control tryptophan and then supplemented with either cysteine or C2 for 3 days. Then, cells were recovered for 1 h in a normal medium (containing C2), subjected to cisplatin treatment for 48 h, and cultured for 3 weeks. This experiment revealed that only the combined treatment of arginine depletion with cysteine stimulated cell survival (Figures 6D and S6F, $p < 0.001$). Cell cultures supplemented with either C2 or control tryptophan depletion, with either C2 or cysteine, showed no survival benefit, denying a key role for the general amino acid deprivation response and free cysteine supplementation in this phenotype (Figures 6D and S6F). We also examined the survival of A549 and A549-KEAP1-WT, deprived of arginine and supplemented with cysteine, to cisplatin treatment. Figure 6E shows that KEAP1-WT expression renders A549 sensitive to this treatment, in line with the KEAP1-WT-mediated repression of genes in the ferroptosis protective pathway (Figure 5I) and the incorporation of R>C substitutants (Figures 5J–5L).

R>C substitutants can potentially promote cell survival following cisplatin treatment in at least two ways. They may stimulate functional alterations in recipient proteins. For example, in Sequestosome 1 (SQSTM1), non-catalytic cysteines link oxidative stress to protein aggregation, autophagy, and cell survival,[50] and in thioredoxin, a protein that protects cells against oxidative stress, structural cysteines that do not participate in the catalytic functions are important for its reactive oxygen-scavenging function.[49] Alternatively, resistance can be a result of a higher cysteine content in the proteome and a better buffering capacity of oxidative stress. To distinguish between these two options, we artificially increased cysteine content in the proteome by ectopically expressing KRT8s(10C)-V5 (where 10 arginine codons were genetically mutated to cysteine). As a control, we used KRT8s(10K)-V5 (where the same 10 arginine residues were
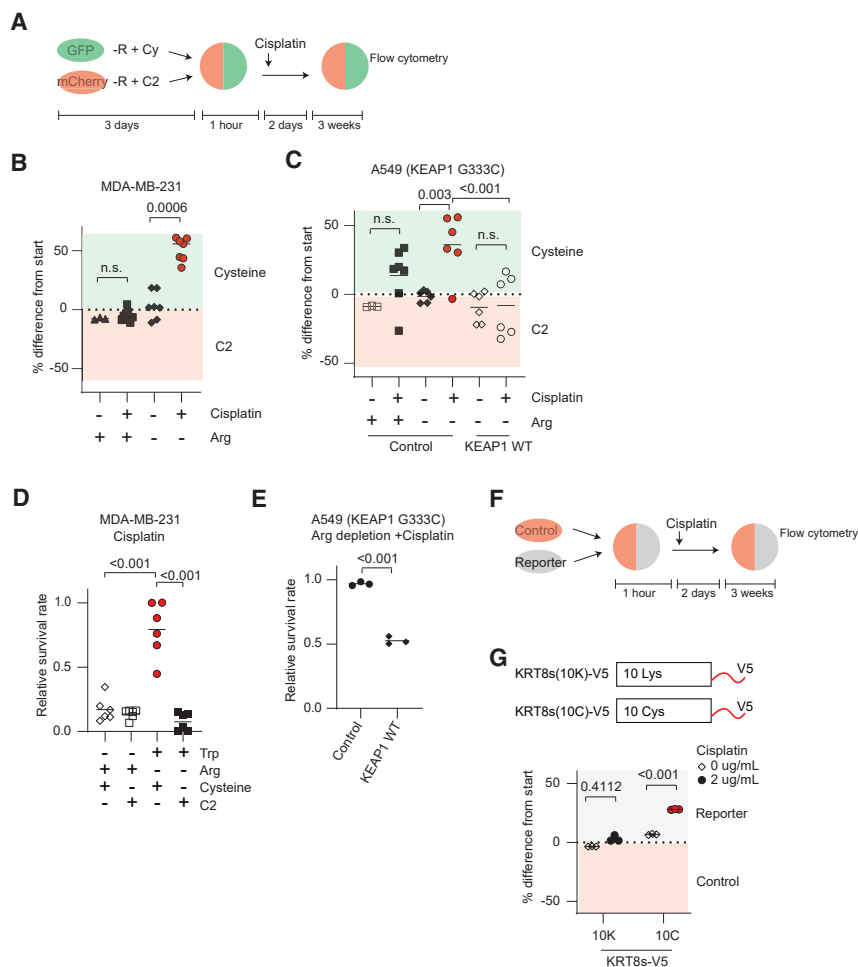
Figure 6. R>C substitutants enhance cellular resistance to chemotherapy

(A) A scheme depicting the setup of the growth-competition assays. −R, Cy, and C2 depict arginine depletion and cysteine and C2 supplementation, respectively.

(B) A dot plot depicting the percent difference in GFP/mCherry signal of MDA-MB-231 cells between 3 weeks and start. The dot plot represents 2–3 independent experiments, and the *p* values were calculated by one-way ANOVA with Sidak's multiple comparisons test.

(C) A dot plot depicting the percent difference in GFP/mCherry signal of A549 control and KEAP1-WT cells between 3 weeks and start. The dot plot represents 3 independent experiments, and the *p* values were calculated by one-way ANOVA with Sidak's multiple comparisons test.

(D) Cell survival experiment using MDA-MB-231 cells, as performed in Figure 6A. *p* values were calculated by one-way ANOVA with Sidak's multiple comparisons test.

(E) Cell survival experiment with A549 and A549-KEAP-WT cells. *p* values were calculated by one-way ANOVA with Sidak's multiple comparisons test.

(F) A scheme depicting growth-competition assays between cells overexpressing the indicated reporter vectors and control cells.

(G) MDA-MB-231 cells containing either KRT8s(10K)-V5 (10K) or KRT8s(10C)-V5 (10C) reporters were treated as indicated and subjected to growth-competition assays as described above (Figure 6F). A reciprocal experiment is presented in Figure S6D. The dot plot represents 3 independent experiments, and the *p* values were calculated by one-way ANOVA with Sidak's multiple comparisons test.

mutated to lysine codons). Immunoblotting analysis verified similar expression of both reporter proteins (Figure S6G). We then first examined the impact of expressing these constructs on the active cysteine assay in cell lysates (see STAR Methods) and observed a substantial average increase of ∼10% (Figure S6H). Subsequently, we subjected these cell populations to a growth-competition assay against cells marked with either a mCherry red fluorescent protein or a GFP (green fluorescent protein) (Figure 6F). Figure 6G shows enhanced survival of the cells containing the KRT8(10C)-V5 reporter vector only when the cells were treated with cisplatin compared with untreated cell populations (*p* < 0.001). We observed this behavior regardless of the competing cells we used (Figure S6I, *p* < 0.001). By contrast, KRT8s(10K)-V5-expressing cells did not show any significant growth advantage in any of the conditions (Figures 6G and S6F). Thus, increasing the portion of cysteine residues in the proteome can explain the enhanced survival of cancer cells to cisplatin treatment upon induction of R>C substitutants.

DISCUSSION

We describe here the identification of R>C codon reassignments (R>C substitutants) in the proteomes of lung cancer patients and

suggest a function for such aberrant mRNA products. The expression of R>C substitutants was enriched in the tumor compartment and linked to oncogenic mutations along the KEAP1-CUL3-NRF2 ferroptosis pathway. We propose that the incorporation of R>C substitutants into cancer proteomes endows cancer cells with more resilience to stress.

Our findings suggest a different perspective on the suppression of arginine production in cancer that may be considered for its therapeutic implications (Figure 7). It has been described that arginine shortage elevates the availability of aspartate to foster pyrimidine production and cancer cell proliferation, and that low arginine levels also limit anti-tumor immunity of tumor-infiltrating T cells.[11,15] Moreover, arginine shortage enforces codon-dependent DNA sequence evolution in colorectal cancer cells.[26] Here, we indicate that intratumoral arginine shortage may also boost resistance to genotoxic stress by boosting cysteine incorporation into proteomes (Figure 7). Cysteine is a key player in cellular protection from oxidative stress.[56] It is the major and limiting factor for producing the antioxidant GSH, and it also directly scavenges free radicals with its thiol group.[57] We suspect that tumors may benefit more from R>C substitutants than either free cysteines or increased production of cysteine-rich proteins. R>C substitutants are likely to be more stable
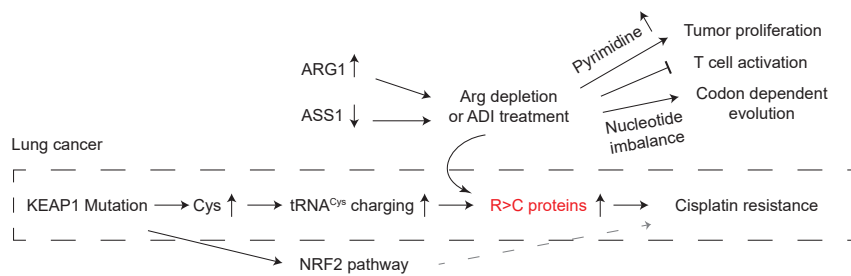
Figure 7. A model cell for arginine shortage benefits in lung cancer
A model depicting the impact of arginine depletion on tumor proliferation, codon-dependent evolution, T cell activity, and resistance to chemotherapy by R>C.

than free cysteines (half-life of ~30 min), are caged intracellularly, and are not likely to be engaged in either catalytic activities or structure formation as most encoded cysteines.

Several threads connect KEAP1 to cysteine. KEAP1 is a cysteine-rich protein, of which a few residues (C151, C226, C273, C288, and C622/624) are oxidized in response to electrophiles, oxidative stimuli, and toxins, linking KEAP1 to redox homeostasis.[58,59] These cysteines are functionally important to control KEAP1 activity, as their modification results in the nuclear accumulation of NRF2 and the induction of downstream target genes involved in antioxidation responses. In addition, NRF2 pathway activation elevates SLC7A11, a glutamine/C2 antiporter,[37–39] and KEAP1 mutations stimulate the accumulation of intracellular cysteine levels.[41] Our results suggest that intracellular cysteine affects tRNA charging during arginine depletion, increasing R>C substitutant events.

Our demonstrations that R>C levels associate with KEAP1 pathway mutations and that KEAP1-WT expression suppresses R>C expression in cells with mutated KEAP1 not only provide another important layer that links KEAP1 to cysteine metabolism but also connect it to lung cancer development and inhibition of arginine production by ASS1 suppression. Moreover, KEAP1 pathway mutations are associated with clinical chemotherapeutic resistance,[60] and NRF2 inhibition sensitizes cells to cisplatin treatment.[61] Our results show that KEAP1-pathway-dependent enrichment of proteomes with cysteines by an R>C mechanism may provide an additional means to balance redox stress during tumor development and cisplatin treatment to allow better survival.

In previous work, we discovered the production of W>F substitutants by tryptophan shortage as the first described regulated codon reassignment event in mammalian systems. The identification of R>C substitutants not only broadens the spectrum of cancer-associated substitutants but also indicates a fundamentally different process and impact. Although W>F substitutants are stimulated in many cancer types by interferon (IFN)γ-mediated IDO1 induction during T cell activation, R>C substitutants arise from a combined effect of arginine shortage and increased cysteine availability in lung cancers with oncogenic mutations associated with ferroptosis protection. Mechanistically, we pinpoint tRNA misalignment as the key causal event of R>C substitutants production, while mis-acylation is the key underlying mechanism of W>F substitutants. Though amino acid shortage-induced tRNA misalignments were described before (e.g., Mordret et al.[29] and Boddapati et al.[62]), our study indicates a functional role of regulatory codon reassignments in human cancer development.

In Figure S6A, we observed that KEAP1-WT expression in KEAP1-mutant A549 cells increased intracellular C2 and cysteine levels. In Figures 5I–5M and 6, we demonstrate that KEAP1-WT expression suppressed SLC7A11, the main C2 transporter, and dramatically suppressed R>C and cisplatin resistance. Although this supports a role for R>C in cell survival, the contradiction between reduced SLC7A11 expression and higher C2 and cysteine levels is puzzling. We speculate that either other transporter proteins mediate C2 and cysteine uptake in acute arginine-deprivation conditions or that KEAP1-WT expression may affect ribosomes to suppress aberrant protein production.

Finally, our results may have consequences for the clinical application of arginine-deprivation therapies by ADI-PEG20 that are being exploited for ASS1-low cancers. We show that ADI treatment stimulates R>C substitutants in cells with low ASS1 expression. As R>C substitutants enhance resistance to cisplatin, and ADI-PEG20 is frequently combined with cisplatin treatment in lung cancer, increased arginine deprivation by ADI-PEG20 may counteract cisplatin-treatment efficacy in tumors with mutations in the KEAP1 pathway.

Limitations of the study

Our study linked R>C substitutants with an arginine-depleted and cysteine-enriched environment in cultured cell conditions but did not connect these events in patient tissues. To address this issue, metabolomics, proteomics, and genomics datasets of lung cancer patients need to be produced and interrogated.

Although we have shown that global enrichment of proteomes with cysteines boosts protection from cisplatin treatment (Figure 6), we did not exclude the potential importance of a few regulatory R>C events and other roles for cysteine in promoting cancer cell survival to cisplatin.

Finally, current mass-spectrometry analysis prevents estimating absolute levels of induced endogenous R>C substitutants. Moreover, various analysis tools may show divergent peptide identifications and have unique biases, excluding the false discovery of individual peptides.

STAR★METHODS

Detailed methods are provided in the online version of this paper and include the following:

- KEY RESOURCES TABLE
- RESOURCE AVAILABILITY
  - Lead contact
  - Materials availability
  - Data and code availability

- EXPERIMENTAL MODEL AND STUDY PARTICIPANT DETAILS
  - Cell-culture and reagents
- METHOD DETAILS
  - Generation of plasmids
  - Lentiviral production and transduction
  - Flow cytometry and DCFDA-Cellular Ros Assay
  - Immunoblotting
  - Active cysteine assay
  - Anti-V5 IP-elution protocol
  - Protein-incorporated cysteine analysis
  - tRNA aminoacylation
  - Immunofluorescence
  - Cell competition assay
  - Cell survival assay
  - Metabolism measurements
  - Generation of Search Database
  - Scanning of Database
  - Retaining arginine substitutions
  - PEPQUERY validation
  - Characterization of R>C Substitutants
  - Proteomics – sample preparation and LC-MS/MS
  - Generation of search database
  - Screening immunoprecipitation–mass (IP/MS) spectrometry data against the databases
  - Screening whole proteome mass spectrometry data for codon-specific R>C substitutants
- QUANTIFICATION AND STATISTICAL ANALYSIS
  - Cys-index analysis
  - Cell competition anslysis
  - Post-scanning analysis for gene-expression correlation and association with genetic mutations
  - Stastics and reproducibility

SUPPLEMENTAL INFORMATION

ACKNOWLEDGMENTS

AUTHOR CONTRIBUTIONS

R.A. conceived and supervised the project and wrote the manuscript. C.Y. conceived the project, designed and performed the experiments, analyzed the data, and wrote the manuscript. A.P. conceived the project, performed the bioinformatics analyses, and wrote the manuscript. X.F. and J.M.N. performed part of the bioinformatics analyses. E.A.Z. and C.R.B. performed and analyzed the metabolomics experiments. O.B.B. performed the mass spectrometry.

DECLARATION OF INTERESTS

The authors declare no competing interests.

REFERENCES

1. Lukey, M.J., Katt, W.P., and Cerione, R.A. (2017). Targeting amino acid metabolism for cancer therapy. Drug Discov. Today 22, 796–804. https://doi.org/10.1016/j.drudis.2016.12.003.

2. Ganjoo, S., Gupta, P., Corbali, H.I., Nanez, S., Riad, T.S., Duong, L.K., Barsoumian, H.B., Masrorpour, F., Jiang, H., Welsh, J.W., and Cortez, M.A. (2023). The role of tumor metabolism in modulating T-Cell activity and in optimizing immunotherapy. Front. Immunol. 14, 1172931. https://doi.org/10.3389/fimmu.2023.1172931.

3. Siska, P.J., and Rathmell, J.C. (2015). T cell metabolic fitness in antitumor immunity. Trends Immunol. 36, 257–264. https://doi.org/10.1016/j.it.2015.02.007.

4. Nakaya, M., Xiao, Y., Zhou, X., Chang, J.H., Chang, M., Cheng, X., Blonska, M., Lin, X., and Sun, S.C. (2014). Inflammatory T cell responses rely on amino acid transporter ASCT2 facilitation of glutamine uptake and mTORC1 kinase activation. Immunity 40, 692–705. https://doi.org/10.1016/j.immuni.2014.04.007.

5. Lemos, H., Huang, L., Prendergast, G.C., and Mellor, A.L. (2019). Immune control by amino acid catabolism during tumorigenesis and therapy. Nat. Rev. Cancer 19, 162–175. https://doi.org/10.1038/s41568-019-0106-z.

6. O'Sullivan, D., and Pearce, E.L. (2015). Targeting T cell metabolism for therapy. Trends Immunol. 36, 71–80. https://doi.org/10.1016/j.it.2014.12.004.

7. Bian, Y., Li, W., Kremer, D.M., Sajjakulnukit, P., Li, S., Crespo, J., Nwosu, Z.C., Zhang, L., Czerwonka, A., Pawłowska, A., et al. (2020). Cancer SLC43A2 alters T cell methionine metabolism and histone methylation. Nature 585, 277–282. https://doi.org/10.1038/s41586-020-2682-1.

8. Guo, C., You, Z., Shi, H., Sun, Y., Du, X., Palacios, G., Guy, C., Yuan, S., Chapman, N.M., Lim, S.A., et al. (2023). SLC38A2 and glutamine signalling in cDC1s dictate anti-tumour immunity. Nature 620, 200–208. https://doi.org/10.1038/s41586-023-06299-8.

9. Werner, A., Amann, E., Schnitzius, V., Habermeier, A., Luckner-Minden, C., Leuchtner, N., Rupp, J., Closs, E.I., and Munder, M. (2016). Induced arginine transport via cationic amino acid transporter-1 is necessary for human T-cell proliferation. Eur. J. Immunol. 46, 92–103. https://doi.org/10.1002/eji.201546047.

10. Rodriguez, P.C., Quiceno, D.G., and Ochoa, A.C. (2007). L-arginine availability regulates T-lymphocyte cell-cycle progression. Blood 109, 1568–1573. https://doi.org/10.1182/blood-2006-06-031856.

11. Geiger, R., Rieckmann, J.C., Wolf, T., Basso, C., Feng, Y., Fuhrer, T., Kogadeeva, M., Picotti, P., Meissner, F., Mann, M., et al. (2016). L-Arginine Modulates T Cell Metabolism and Enhances Survival and Anti-tumor Activity. Cell 167, 829–842.e13. https://doi.org/10.1016/j.cell.2016.09.031.

12. Huang, H.Y., Wu, W.R., Wang, Y.H., Wang, J.W., Fang, F.M., Tsai, J.W., Li, S.H., Hung, H.C., Yu, S.C., Lan, J., et al. (2013). ASS1 as a novel tumor suppressor gene in myxofibrosarcomas: aberrant loss via epigenetic DNA methylation confers aggressive phenotypes, negative prognostic impact, and therapeutic relevance. Clin. Cancer Res. 19, 2861–2872. https://doi.org/10.1158/1078-0432.CCR-12-2641.

13. Sun, N., and Zhao, X. (2022). Argininosuccinate synthase 1, arginine deprivation therapy and cancer management. Front. Pharmacol. 13, 935553. https://doi.org/10.3389/fphar.2022.935553.

14. Carpentier, J., Pavlyk, I., Mukherjee, U., Hall, P.E., and Szlosarek, P.W. (2022). Arginine Deprivation in SCLC: Mechanisms and Perspectives for Therapy. Lung Cancer (Auckl) 13, 53–66. https://doi.org/10.2147/LCTT.S335117.

15. Rabinovich, S., Adler, L., Yizhak, K., Sarver, A., Silberman, A., Agron, S., Stettner, N., Sun, Q., Brandis, A., Helbling, D., et al. (2015). Diversion of aspartate in ASS1-deficient tumours fosters de novo pyrimidine synthesis. Nature 527, 379–383. https://doi.org/10.1038/nature15529.

16. Sullivan, M.R., Danai, L.V., Lewis, C.A., Chan, S.H., Gui, D.Y., Kunchok, T., Dennstedt, E.A., Vander Heiden, M.G., and Muir, A. (2019). Quantification of microenvironmental metabolites in murine cancers reveals determinants of tumor nutrient availability. eLife 8, e44235. https://doi.org/10.7554/eLife.44235.

17. Niu, F., Yu, Y., Li, Z., Ren, Y., Li, Z., Ye, Q., Liu, P., Ji, C., Qian, L., and Xiong, Y. (2022). Arginase: An emerging and promising therapeutic target for cancer treatment. Biomed. Pharmacother. 149, 112840. https://doi.org/10.1016/j.biopha.2022.112840.

18. Rodriguez, P.C., Ochoa, A.C., and Al-Khami, A.A. (2017). Arginine Metabolism in Myeloid Cells Shapes Innate and Adaptive Immunity. Front. Immunol. 8, 93. https://doi.org/10.3389/fimmu.2017.00093.

19. Shimobayashi, M., and Hall, M.N. (2016). Multiple amino acid sensing inputs to mTORC1. Cell Res. 26, 7–20. https://doi.org/10.1038/cr.2015.146.

20. Bartok, O., Pataskar, A., Nagel, R., Laos, M., Goldfarb, E., Hayoun, D., Levy, R., Körner, P.R., Kreuger, I.Z.M., Champagne, J., et al. (2021). Anti-tumour immunity induces aberrant peptide presentation in melanoma. Nature 590, 332–337. https://doi.org/10.1038/s41586-020-03054-1.

21. Rudnick, P.A., Markey, S.P., Roth, J., Mirokhin, Y., Yan, X., Tchekhovskoi, D.V., Edwards, N.J., Thangudu, R.R., Ketcham, K.A., Kinsinger, C.R., et al. (2016). A Description of the Clinical Proteomic Tumor Analysis Consortium (CPTAC) Common Data Analysis Pipeline. J. Proteome Res. 15, 1023–1032. https://doi.org/10.1021/acs.jproteome.5b01091.

22. da Veiga Leprevost, F., Haynes, S.E., Avtonomov, D.M., Chang, H.Y., Shanmugam, A.K., Mellacheruvu, D., Kong, A.T., and Nesvizhskii, A.I. (2020). Philosopher: a versatile toolkit for shotgun proteomics data analysis. Nat. Methods 17, 869–870. https://doi.org/10.1038/s41592-020-0912-y.

23. Wen, B., and Zhang, B. (2023). PepQuery2 democratizes public MS proteomics data for rapid peptide searching. Nat. Commun. 14, 2213. https://doi.org/10.1038/s41467-023-37462-4.

24. Alexandrov, L.B., Kim, J., Haradhvala, N.J., Huang, M.N., Tian Ng, A.W., Wu, Y., Boot, A., Covington, K.R., Gordenin, D.A., Bergstrom, E.N., et al. (2020). The repertoire of mutational signatures in human cancer. Nature 578, 94–101. https://doi.org/10.1038/s41586-020-1943-3.

25. Tsuber, V., Kadamov, Y., Brautigam, L., Berglund, U.W., and Helleday, T. (2017). Mutations in Cancer Cause Gain of Cysteine, Histidine, and Tryptophan at the Expense of a Net Loss of Arginine on the Proteome Level. Biomolecules 7, 49. https://doi.org/10.3390/biom7030049.

26. Hsu, D.J., Gao, J., Yamaguchi, N., Pinzaru, A., Wu, Q., Mandayam, N., Liberti, M., Heissel, S., Alwaseem, H., Tavazoie, S., and Tavazoie, S.F. (2023). Arginine limitation drives a directed codon-dependent DNA sequence evolution response in colorectal cancer cells. Sci. Adv. 9, eade9120. https://doi.org/10.1126/sciadv.ade9120.

27. Satpathy, S., Krug, K., Jean Beltran, P.M., Savage, S.R., Petralia, F., Kumar-Sinha, C., Dou, Y., Reva, B., Kane, M.H., Avanessian, S.C., et al. (2021). A proteogenomic portrait of lung squamous cell carcinoma. Cell 184, 4348–4371.e40. https://doi.org/10.1016/j.cell.2021.07.016.

28. Wong, H.E., Huang, C.J., and Zhang, Z. (2018). Amino Acid Misincorporation Propensities Revealed through Systematic Amino Acid Starvation. Biochemistry 57, 6767–6779. https://doi.org/10.1021/acs.biochem.8b00976.

29. Mordret, E., Dahan, O., Asraf, O., Rak, R., Yehonadav, A., Barnabas, G.D., Cox, J., Geiger, T., Lindner, A.B., and Pilpel, Y. (2019). Systematic Detection of Amino Acid Substitutions in Proteomes Reveals Mechanistic Basis of Ribosome Errors and Selection for Translation Fidelity. Mol. Cell 75, 427–441.e5. https://doi.org/10.1016/j.molcel.2019.06.041.

30. Cheng, C.T., Qi, Y., Wang, Y.C., Chi, K.K., Chung, Y., Ouyang, C., Chen, Y.R., Oh, M.E., Sheng, X., Tang, Y., et al. (2018). Arginine starvation kills tumor cells through aspartate exhaustion and mitochondrial dysfunction. Commun. Biol. 1, 178. https://doi.org/10.1038/s42003-018-0178-4.

31. Pataskar, A., Champagne, J., Nagel, R., Kenski, J., Laos, M., Michaux, J., Pak, H.S., Bleijerveld, O.B., Mordente, K., Navarro, J.M., et al. (2022). Tryptophan depletion results in tryptophan-to-phenylalanine substitutants. Nature 603, 721–727. https://doi.org/10.1038/s41586-022-04499-2.

32. Stockwell, B.R., Friedmann Angeli, J.P., Bayir, H., Bush, A.I., Conrad, M., Dixon, S.J., Fulda, S., Gascón, S., Hatzios, S.K., Kagan, V.E., et al. (2017). Ferroptosis: A Regulated Cell Death Nexus Linking Metabolism, Redox Biology, and Disease. Cell 171, 273–285. https://doi.org/10.1016/j.cell.2017.09.021.

33. Cancer; Genome; Atlas; Research Network (2012). Comprehensive genomic characterization of squamous cell lung cancers. Nature 489, 519–525. https://doi.org/10.1038/nature11404.

34. Tang, D., Chen, X., Kang, R., and Kroemer, G. (2021). Ferroptosis: molecular mechanisms and health implications. Cell Res. 31, 107–125. https://doi.org/10.1038/s41422-020-00441-1.

35. Dodson, M., Castro-Portuguez, R., and Zhang, D.D. (2019). NRF2 plays a critical role in mitigating lipid peroxidation and ferroptosis. Redox Biol. 23, 101107. https://doi.org/10.1016/j.redox.2019.101107.

36. Capece, D., Verzella, D., Flati, I., Arboretto, P., Cornice, J., and Franzoso, G. (2022). NF-κB: blending metabolism, immunity, and inflammation. Trends Immunol. 43, 757–775. https://doi.org/10.1016/j.it.2022.07.004.

37. Dixon, S.J., Lemberg, K.M., Lamprecht, M.R., Skouta, R., Zaitsev, E.M., Gleason, C.E., Patel, D.N., Bauer, A.J., Cantley, A.M., Yang, W.S., et al. (2012). Ferroptosis: an iron-dependent form of nonapoptotic cell death. Cell 149, 1060–1072. https://doi.org/10.1016/j.cell.2012.03.042.

38. Jiang, L., Kon, N., Li, T., Wang, S.J., Su, T., Hibshoosh, H., Baer, R., and Gu, W. (2015). Ferroptosis as a p53-mediated activity during tumour suppression. Nature 520, 57–62. https://doi.org/10.1038/nature14344.

39. Habib, E., Linher-Melville, K., Lin, H.X., and Singh, G. (2015). Expression of xCT and activity of system xc(-) are regulated by NRF2 in human breast cancer cells in response to oxidative stress. Redox Biol. 5, 33–42. https://doi.org/10.1016/j.redox.2015.03.003.

40. Koppula, P., Zhuang, L., and Gan, B. (2021). Cystine transporter SLC7A11/xCT in cancer: ferroptosis, nutrient dependency, and cancer therapy. Protein Cell 12, 599–620. https://doi.org/10.1007/s13238-020-00789-5.

41. Kang, Y.P., Torrente, L., Falzone, A., Elkins, C.M., Liu, M., Asara, J.M., Dibble, C.C., and DeNicola, G.M. (2019). Cysteine dioxygenase 1 is a metabolic liability for non-small cell lung cancer. eLife 8, e45572. https://doi.org/10.7554/eLife.45572.

42. Chan, P.Y., Phillips, M.M., Ellis, S., Johnston, A., Feng, X., Arora, A., Hay, G., Cohen, V.M.L., Sagoo, M.S., Bomalaski, J.S., et al. (2022). A Phase 1 study of ADI-PEG20 (pegargiminase) combined with cisplatin and pemetrexed in ASS1-negative metastatic uveal melanoma. Pigment Cell Melanoma Res. 35, 461–470. https://doi.org/10.1111/pcmr.13042.

43. Yao, S., Janku, F., Koenig, K., Tsimberidou, A.M., Piha-Paul, S.A., Shi, N., Stewart, J., Johnston, A., Bomalaski, J., Meric-Bernstam, F., and Fu, S. (2022). Phase 1 trial of ADI-PEG 20 and liposomal doxorubicin in patients with metastatic solid tumors. Cancer Med. 11, 340–347. https://doi.org/10.1002/cam4.4446.

44. Szlosarek, P.W., Wimalasingham, A.G., Phillips, M.M., Hall, P.E., Chan, P.Y., Conibear, J., Lim, L., Rashid, S., Steele, J., Wells, P., et al. (2021). Phase 1, pharmacogenomic, dose-expansion study of pegargiminase plus pemetrexed and cisplatin in patients with ASS1-deficient non-squamous non-small cell lung cancer. Cancer Med. 10, 6642–6652. https://doi.org/10.1002/cam4.4196.

45. Tsai, H.J., Hsiao, H.H., Hsu, Y.T., Liu, Y.C., Kao, H.W., Liu, T.C., Cho, S.F., Feng, X., Johnston, A., Bomalaski, J.S., et al. (2021). Phase I study of ADI-PEG20 plus low-dose cytarabine for the treatment of acute myeloid leukemia. Cancer Med. 10, 2946–2955. https://doi.org/10.1002/cam4.3871.

46. Hall, P.E., Ready, N., Johnston, A., Bomalaski, J.S., Venhaus, R.R., Sheaff, M., Krug, L., and Szlosarek, P.W. (2020). Phase II Study of Arginine Deprivation Therapy With Pegargiminase in Patients With Relapsed Sensitive or Refractory Small-cell Lung Cancer. Clin. Lung Cancer 21, 527–533. https://doi.org/10.1016/j.cllc.2020.07.012.

47. Hall, P.E., Lewis, R., Syed, N., Shaffer, R., Evanson, J., Ellis, S., Williams, M., Feng, X., Johnston, A., Thomson, J.A., et al. (2019). A Phase I Study of Pegylated Arginine Deiminase (Pegargiminase), Cisplatin, and Pemetrexed in Argininosuccinate Synthetase 1-Deficient Recurrent High-grade Glioma. Clin. Cancer Res. *25*, 2708–2716. https://doi.org/10.1158/1078-0432.CCR-18-3729.

48. Abou-Alfa, G.K., Qin, S., Ryoo, B.Y., Lu, S.N., Yen, C.J., Feng, Y.H., Lim, H.Y., Izzo, F., Colombo, M., Sarker, D., et al. (2018). Phase III randomized study of second line ADI-PEG 20 plus best supportive care versus placebo plus best supportive care in patients with advanced hepatocellular carcinoma. Ann. Oncol. *29*, 1402–1408. https://doi.org/10.1093/annonc/mdy101.

49. Das, K.C., and Das, C.K. (2000). Thioredoxin, a singlet oxygen quencher and hydroxyl radical scavenger: redox independent functions. Biochem. Biophys. Res. Commun. *277*, 443–447. https://doi.org/10.1006/bbrc.2000.3689.

50. Carroll, B., Otten, E.G., Manni, D., Stefanatos, R., Menzies, F.M., Smith, G.R., Jurk, D., Kenneth, N., Wilkinson, S., Passos, J.F., et al. (2018). Oxidation of SQSTM1/p62 mediates the link between redox state and protein homeostasis. Nat. Commun. *9*, 256. https://doi.org/10.1038/s41467-017-02746-z.

51. Ishii, T., and Bannai, S. (1985). The synergistic action of the copper chelator bathocuproine sulphonate and cysteine in enhancing growth of L1210 cells in vitro. J. Cell. Physiol. *125*, 151–155. https://doi.org/10.1002/jcp.1041250119.

52. Zhang, X., Sui, S., Wang, L., Li, H., Zhang, L., Xu, S., and Zheng, X. (2020). Inhibition of tumor propellant glutathione peroxidase 4 induces ferroptosis in cancer cells and enhances anticancer effect of cisplatin. J. Cell. Physiol. *235*, 3425–3437. https://doi.org/10.1002/jcp.29232.

53. Tian, Y., Wu, K., Liu, Q., Han, N., Zhang, L., Chu, Q., and Chen, Y. (2016). Modification of platinum sensitivity by KEAP1/NRF2 signals in non-small cell lung cancer. J. Hematol. Oncol. *9*, 83. https://doi.org/10.1186/s13045-016-0311-0.

54. Wang, X.J., Sun, Z., Villeneuve, N.F., Zhang, S., Zhao, F., Li, Y., Chen, W., Yi, X., Zheng, W., Wondrak, G.T., et al. (2008). Nrf2 enhances resistance of cancer cells to chemotherapeutic drugs, the dark side of Nrf2. Carcinogenesis *29*, 1235–1243. https://doi.org/10.1093/carcin/bgn095.

55. Jeong, Y., Hellyer, J.A., Stehr, H., Hoang, N.T., Niu, X., Das, M., Padda, S.K., Ramchandran, K., Neal, J.W., Wakelee, H., and Diehn, M. (2020). Role of KEAP1/NFE2L2 Mutations in the Chemotherapeutic Response of Patients with Non-Small Cell Lung Cancer. Clin. Cancer Res. *26*, 274–281. https://doi.org/10.1158/1078-0432.CCR-19-1237.

56. Lee, J., and Roh, J.L. (2022). SLC7A11 as a Gateway of Metabolic Perturbation and Ferroptosis Vulnerability in Cancer. Antioxidants (Basel) *11*, 2444. https://doi.org/10.3390/antiox11122444.

57. Forman, H.J., Zhang, H., and Rinna, A. (2009). Glutathione: overview of its protective roles, measurement, and biosynthesis. Mol. Aspects Med. *30*, 1–12. https://doi.org/10.1016/j.mam.2008.08.006.

58. Suzuki, T., Takahashi, J., and Yamamoto, M. (2023). Molecular Basis of the KEAP1-NRF2 Signaling Pathway. Mol. Cells *46*, 133–141. https://doi.org/10.14348/molcells.2023.0028.

59. Pillai, R., Hayashi, M., Zavitsanou, A.M., and Papagiannakopoulos, T. (2022). NRF2: KEAPing Tumors Protected. Cancer Discov. *12*, 625–643. https://doi.org/10.1158/2159-8290.CD-21-0922.

60. Islam, S.S., Qassem, K., Islam, S., Parag, R.R., Rahman, M.Z., Farhat, W.A., Yeger, H., Aboussekhra, A., Karakas, B., and Noman, A.S.M. (2022). Genetic alterations of Keap1 confers chemotherapeutic resistance through functional activation of Nrf2 and Notch pathway in head and neck squamous cell carcinoma. Cell Death Dis. *13*, 696. https://doi.org/10.1038/s41419-022-05126-8.

61. Zhang, D., Hou, Z., Aldrich, K.E., Lockwood, L., Odom, A.L., and Liby, K.T. (2021). A Novel Nrf2 Pathway Inhibitor Sensitizes Keap1-Mutant Lung Cancer Cells to Chemotherapy. Mol. Cancer Ther. *20*, 1692–1701. https://doi.org/10.1158/1535-7163.MCT-21-0210.

62. Boddapati, S., Gilmore, J., Boone, K., Bushey, J., Ross, J., Gfeller, B., McFee, W., Rao, R., Corrigan, G., Chen, A., et al. (2020). Evidence for co-translational misincorporation of non-canonical amino acid hydroxy-proline in recombinant antibodies produced in Chinese Hamster Ovary (CHO) cell lines. PLoS One *15*, e0241250. https://doi.org/10.1371/journal.pone.0241250.

63. Champagne, J., Pataskar, A., Blommaert, N., Nagel, R., Wernaart, D., Ramalho, S., Kenski, J., Bleijerveld, O.B., Zaal, E.A., Berkers, C.R., et al. (2021). Oncogene-dependent sloppiness in mRNA translation. Mol. Cell *81*, 4709–4721.e9. https://doi.org/10.1016/j.molcel.2021.09.002.

64. Perez-Riverol, Y., Bai, J., Bandla, C., García-Seisdedos, D., Hewapathirana, S., Kamatchinathan, S., Kundu, D.J., Prakash, A., Frericks-Zipper, A., Eisenacher, M., et al. (2022). The PRIDE database resources in 2022: a hub for mass spectrometry-based proteomics evidences. Nucleic Acids Res. *50*, D543–D552. https://doi.org/10.1093/nar/gkab1038.

65. Tyanova, S., Temu, T., and Cox, J. (2016). The MaxQuant computational platform for mass spectrometry-based shotgun proteomics. Nat. Protoc. *11*, 2301–2319. https://doi.org/10.1038/nprot.2016.136.

66. Perez-Riverol, Y., Csordas, A., Bai, J., Bernal-Llinares, M., Hewapathirana, S., Kundu, D.J., Inuganti, A., Griss, J., Mayer, G., Eisenacher, M., et al. (2019). The PRIDE database and related tools and resources in 2019: improving support for quantification data. Nucleic Acids Res. *47*, D442–D450. https://doi.org/10.1093/nar/gky1106.

CellPress
OPEN ACCESS

STAR★METHODS

KEY RESOURCES TABLE

REAGENT or RESOURCE	SOURCE	IDENTIFIER
Antibodies		
Mouse anti V5 tag monoclonal	Invitrogen	Catalog # R960-25; RRID: AB_2556564
rabbit anti-ASS1	Proteintech	Catalog# 16210-1-AP; RRID:AB_2060466
Mouse anti-HSP90	BD bioscience	Catalog # 610418; RRID: AB_397798
rat anti-tubulin	Santa Cruz	Catalog # sc-53029; RRID: AB_793541
Rabbit anti-RARS	Proteintech	Catalog # 27344-1-AP; RRID:AB_2880849
Rb anti-phospho-eIF2a	Cell signaling	3398
IRDye 680RD donkey anti-mouse	LI-COR	Catalog # 926-68072; RRID: AB_10953628
IRDye 800CW goat anti-rabbit	LICOR	Catalog # 926-32211; RRID: AB_621843
IRDye 800RD goat anti-rat	LI-COR	Catalog # 926-32219; RRID: AB_1850025
Bacterial and virus strains		
DH5-alpha	Thermo Fisher Scientific	Catalog# 18265017
Chemicals, peptides, and recombinant proteins		
T4 RNA Ligase 2 (dsRNA Ligase)	New England biolabs	Catalog #M0239L
Zeba Spin Desalting Columns, 7K MWCO, 0.5 mL	Thermo Fisher scientific	Catalog # 89883
BCA Protein Assay Kit	Thermo Fisher Scientific	Catalog # 23225
Blasticidin S Hydrochloride	Thermo Fisher Scientific	Catalog # 10264913
Crystal violet solution	Sigma Aldrich	Catalog # V5265
DAPI (4',6-Diamidino-2-Phenylindole, Dihydrochloride)	Thermo Fisher Scientific	Catalog # D1306
Dulbecco's MEM (DMEM) F-12 w/o Tryptophan	USBiological life Sciences	Catalog # D9807-04-10
Fetal Bovine Serum, dialyzed US origin	Thermo Fisher Scientific	Catalog # 26400044
Formaldehyde solution	Sigma Aldrich	Catalog # 252549
Gibco HEPES (1M)	Thermo Fisher Scientific	Catalog # 15630056 or # 15630-080
GlutaMAX Supplement	Thermo Fisher Scientific	Catalog # 35050038
Sodium bicarbonate	Sigma Aldrich	Catalog # S6014
Trizol	Thermo Fisher Scientific	Catalog # 15596018
Tween 20	Sigma Aldrich	Catalog # P1379
Phusion HF DNA Polymerase	Thermo Fisher Scientific	Catalog # F530
Polyethylenimine Hydrochloride	Polysciences	Catalog # 25439-2
Puromycin	Bio-connect	Catalog # AG-CN2-0078-M500
ChromoTek V5-Trap Magnetic Agarose	proteintech	Catalog # v5tma-20
Sodium acetate, 1M aq. soln., pH 4.5	Santa Cruz	sc-296390
Glucose solution	Sigma	49163-100ML
Amersham MicroSpin G-50 Columns	Cytivalifesciences	Catalog # 27533001
Acid-Phenol:Chloroform, pH 4.5 (with IAA, 125:24:1)	Thermo Fisher Scientific	Catalog # AM9720
(+)-Biotin-(PEO)3-iodoacetamide	Santa Cruz	Catalog # sc-470524A
Pemetrexed (LY-231514) disodium	Selleckchem	Catalog # S1135
DY-547P1-Maleimide	dyomics	Catalog # 547P1-03
V5 peptide	chromotek	Catalog # v5p-1
Critical commercial assays		
EZ-PCR Mycoplasma Detection Kit	Biological Industries	Catalog # 20-700-20
PureLink Quick Midiprep Kit	Thermo Fisher Scientific	Catalog # K210004
PureLink Quick Miniprep Kit	Thermo Fisher Scientific	Catalog # K210002
SensiFAST SYBR No-ROX Kit	Bioline	Catalog # BIO-98050

Continued

REAGENT or RESOURCE	SOURCE	IDENTIFIER
SuperScript III Reverse Transcriptase	Thermo Fisher Scientific	Catalog # 18080093
Wizard SV Gel and PCR Clean-Up System	Promega	Catalog # A9282
Deposited data		
Mass spectrometry proteomics	This study	Pride: PXD043612
Philosopher parameters	This study	https://doi.org/10.17632/3wfxrz66w2.1
Western blot	This study	https://doi.org/10.17632/bvdn865y9c.1
LSCC proteome	CPTAC	PDC000234
CCRCC proteome	CPTAC	PDC000127
GBM proteome	CPTAC	PDC000204
HNSCC proteome	CPTAC	PDC000221
HCC proteome	CPTAC	PDC000198
OVSCC proteome	CPTAC	PDC000110
PDA proteome	CPTAC	PDC000270
UCEC proteome	CPTAC	PDC000125
LUAD proteome	CPTAC	PDC000153
Experimental models: Cell lines		
293T	Internal stock	RRID:CVCL_0063
A549	Internal stock	RRID:CVCL_0023
MDA-MB-231	Internal stock	RRID:CVCL_0062
Oligonucleotides		
ON-TARGETplus Human RARS siRNA	horizon discovery	LQ-009820-02-0002
Recombinant DNA		
pCDH- KRT8S	This study	N/A
pTeton-KRT8s	This study	N/A
pLX304-KRT8s	This study	N/A
pCDH- KRT8S R>K	This study	N/A
pCDH- KRT8S 10R>10C	This study	N/A
pCDH- KRT8S 10R>10K	This study	N/A
pCDH- KRT8S agg	This study	N/A
pCDH- KRT8S cgc	This study	N/A
pCDH- KRT8S cgg	This study	N/A
pCDH- KRT8S agt	This study	N/A
pCDH-KEAP1	This study	N/A
Software and algorithms		
Philosopher 4.0.0	NesviLab	https://github.com/Nesvilab/philosopher/releases
Philosopher 5.0	NesviLab	https://github.com/Nesvilab/philosopher/releases
PEPQUERY2	Pepquery.org	http://www.pepquery.org/
Adobe Illustrator CC 2017	Adobe acrobat	http://www.adobe.com
ImageJ	NIH	https://imagej.nih.gov/ij/
FlowJo V10 software (FlowJo)	FlowJo	https://www.flowjo.com/
TraceFinder software	Thermo Fisher Scientific	https://www.thermofisher.com/
Prism9	GraphPad software	https://www.graphpad.com/scientific-software/prism/

RESOURCE AVAILABILITY

Lead contact

Further information and requests for resources and reagents should be directed to and will be fulfilled by the lead contact Reuven Agami (r.agami@nki.nl)

Materials availability

All strains generated in this study are available without restriction upon request

Data and code availability

- In this study, a comprehensive dataset was assembled, comprising in total of 911 tumor tissues and 558 adjacent normal tissues across multiple cancer types. The Dataset was assembled from PDC commons (https://pdc.cancer.gov/pdc/), and the PDC IDs are reported in the key resources table (above). The Mass spectrometry proteomics data have been deposited at Pride, and original western blot images have been deposited in Mendeley, all will be publicly available as of the date of publication. The DOI is listed in the key resources table.
- All original codes have been deposited at Mendeley Data and are publicly available as of the date of publication. DOIs are listed in the key resources table.
- Any additional information required to reanalyze the data reported in the paper is available from the lead contact upon request.

EXPERIMENTAL MODEL AND STUDY PARTICIPANT DETAILS

Cell-culture and reagents

MDA-MB-231, HEK 293T, A549, and MCF-7 were cultured in Dulbecco's modified Eagle's medium (DMEM, Gibco), supplemented with 10% fetal bovine serum and 100 U/ml penicillin/streptomycin. All cells were maintained in 5% CO_2 humidified incubator at 37°C. Before transfection, cells were seeded on 6-well plates and grown to 50-70% confluency. All cell lines were purchased for ATCC and tested (PCR) negative for mycoplasma contamination.

Arginine, cystine (C2), and tryptophan-free DMEM media were custom-made (Cell Culture Technology), supplemented with 10% heat-inactivated and dialyzed fetal bovine serum (Gibco), and 100 U/ml penicillin/streptomycin. L-cysteine (sigma, C6852) and L-cystine (Alfa Aesar, J62292) were prepared in PBS, and used at a final concentration of 200 uM. Polyethylenimine (PEI, Polysciences) was dissolved in water at a concentration of 1 mg/mL.

METHOD DETAILS

Generation of plasmids

Keratin 8 amino acids 205-483 (KRT8s-V5: UniProt: P05787) was obtained by PCR from CCSB-Broad Lentiviral Expression Library, and was used as a template to construct the KRT8s-V5 reporter vector. Primers listed in Table S7 were used for PCR, and DNA fragments were cloned into pCDH vector by Gibson assembly at XbaI and NotI sites. The KRT8s(R>K)-V5, KRT8s(R>C)-V5, KRT8s(AGG)-V5, KRT8s(CGC)-V5, KRT8s(10K)-V5, and KRT8s(10C)-V5 were synthesis from gblock fragments (IDT) and cloned in the same way as mentioned above. KEAP1-WT cDNA was cloned into the pX304-Blast vector.

Lentiviral production and transduction

For lentivirus production, 4 million per 10 cm dish HEK 293T cells were seeded one day prior to transfection. For each transfection, 500 μl of serum-free opti MEM added 63 μl of 1 mg/ml PEI solution. Another 500 uL of serum-free opti MEM added 10 μg of the pCDH vector of interest, 5 μg of pMDL RRE, 3.5 μg pVSV-G AND 2.5 μg of pRSV-REV plasmids. Next, the two media were combined to make 1mL, mixture by vortex. Then, the mixture was incubated for 15 min at room temperature and applied to the HEK 293T cells. After overnight incubation, the medium was replaced, and the lentivirus-containing supernatants were collected 72h after transfection, snap frozen in liquid nitrogen, and preserved in -80 freezer.

Target cells were transduced by supplementation of the lentiviral supernatant with 8 μg/ml polybrene (Sigma). One day after transduction, the transduced cells were selected by either the addition of 5 μg/ml Blasticidin (Invitrogen), 2 μg/ml puromycin (Gibco) or sorted by FACS.

Flow cytometry and DCFDA-Cellular Ros Assay

Cells were incubated with 10 uM DCFH-DA (35845, Sigma) for 30 min, then washed and collected by trypsinization, then the cells were resuspended in PBS after centrifugation. Single live cells were selected by forward scattering and side scattering, and DAPI staining. Then cells were analyzed on an LSR Fortessa (BD) and the results were analyzed using FlowJo V10 software (FlowJo).

Immunoblotting

All cells were washed with PBS and collected by trypsinization. Cells were lysis on ice for 15 min with lysis buffer containing 25mM Tris HCl, PH7.5, 250mM NaCl, 1%NP-40, 1mM EDTA, 5% glycerol and freshly added protease inhibitor (Roche, 11836145001). Then supernatants were collected after centrifuging for 12,000g at 4 °C for 10 min. For western blot, samples were prepared by adding 4x Laemmli buffer and heated on a metal bath for 5 min. Then the samples are ready to run on SDS-PAGE gel or preserved at -20 freezer. 22 μm pore size nitrocellulose membranes (Santa Cruz) were used for western blot. Mouse anti V5 tag monoclonal antibodies (Invitrogen, R960-25; 1:1,000), rabbit anti-ASS1 (proteintech, 16210-1-AP; 1;2000), Mouse anti-HSP90 (BD, 610418; 1:2000) rat

anti-tubulin (Santa Cruz, SC-53029; 1:5000) and Rb anti-phospho-eIF2a (Cell signaling, 3398) were used to stain the corresponding proteins. Secondary antibody stainings were performed with IRDye 680RD donkey anti-mouse (LI-COR, 926-68072, 1:10,000) and IRDye 800CW goat anti-rabbit (LI-COR, 926-32211, 1:10,000) IRDye 680RD goat anti-rat (LI-COR, 926-68076; 1:10 000). Visualization was performed by use of an Odyssey infrared scanning device (LI-COR).

Active cysteine assay

Cells were lysed as described above. Cellular debris was removed by centrifugation at 12000 g for 15 min at 4 °C. Lysates were then incubated on ice for 30 min with 10 mM biotinylated (peo3) iodoacetamide (sc-470524A, Santa Cruz) to label free thiol group labeling, Samples were then used for western blot.

Anti-V5 IP-elution protocol

Cells were lysis as mentioned above and centrifuged, and the supernatant was collected and cocultured with prewashed V5 magnetic beads (Proteintech, v5tma) for 1.5 hours at 4 °C on a rotor. The beads were washed 5 times with wash buffer: PBS containing 1% triton x-100, 250mM NaCl, 50mM HEPES, PH7.5, 1mM MgCl$_2$ supplemented with protease inhibitor (Roche). Then, proteins on the beads were eluted with V5 peptides (1 mg/mL) for 20 min at 37 °C on a vortex mixture. The eluted proteins were sent for either mass spectrometry analysis or cysteine content analysis.

Protein-incorporated cysteine analysis

The eluted proteins from the Anti-V5 IP-elution protocol were treated with DTT for 20 min at room temperature. Meantime, the Zeba Spin Desalting Columns (Thermo 89883) were washed 3 times with wash buffer. Then the DTT was removed by loading the solution on the desalting columns. The elution was then stained with 10 uM maleimide (dyomics, 547P1-03) for 20 min at room temperature on a rotor. Cysteine maleimide samples were prepared after 4x Laemmli buffer was added and boiled for 5 min on a metal bath. Protein samples were either separated on SDS-PAGE gel or preserved at -20 °C freezer.

To quantify the content of cysteine in the reporter proteins, samples with similar amounts were loaded and separated on two SDS-PAGE gels, one was used for immunoblotting analysis to examine the total amount of V5 purified protein, another for the cysteine detection on the gel by Typhoon FLA9500 (GE). For cysteine detection, in brief, SDS-PAGE gels were fixed by 10% acetic acid for 30 min, washed 5 times with water every 10 min, then fluorescent was scanned on Typhoon FLA9500 by TAMRA channel.

tRNA aminoacylation

Cells were seeded in 10 cm dish and harvested in cold PBS, centrifuged, and resuspended in 500uL ice-cold lysis buffer containing 0.3 M sodium acetate/acetic acid (NaOAc/HOAc) at pH 4.5 and 10mM EDTA. Total RNA was isolated using acetate-saturated phenol/CHCl3 (pH 4.5). Precipitated RNA was resuspended in 40uL 10 mM NaOAc/HOAc (pH 4.5). Samples were split into two, one half (about 2 μg) was oxidized with 50 mM NaIO4 in 100 mM NaOAc/HOAc (pH 4.5) for 30 min and the other half (∼ 2 μg) was incubated in 50 mM NaCl in 100 mM NaOAc/HOAc (pH 4.5) for 30 min. Samples were quenched with glucose 100 mM for 5 min at room temperature, purified in G50 columns ((27533001, cytivalifesciences), and then precipitated with ethanol. tRNAs were deacylated in 50 mM Tris-HCl (pH 9) for 30 min at 37 °C. RNA was precipitated and then ligated to the 3′adaptor (5′-/5rApp/ TGGAATTCTCGGGTGCCAAGG/3ddC/-3′) using T4 RNA ligase 2 (M0239 NEB) for 1 h at 25 °C and 1 h at 37 °C. and then precipitated with ethanol. Super Script III RT kit (Invitrogen) and Reverse primer, GCCTTGGCACCCGAGAATTCCA were used for Reverse transcription, then the product can be stored in -20 °C freezer.

Relative aminoacylation levels were calculated by qRT–PCR using tRNA specific primers.

Reverse primer, GCCTTGGCACCCGAGAATTCCA; Arg-tRNA(ACG) primer, GGGCCAGTGGCGCAATGGATAA; Arg-tRNA(CCG) primer, GGCCGCGTGGCCTAATGGATAA; Cys-tRNA(GCA-2) primer, GGGGGTATAGCTCAGTGGTAGA; Cys-tRNA(GCA-3) primer, GGGGGTATAGCTCAGGGGTAGA; Pro-tRNA(AGG) primer, GGCTCGTTGGTCTAGGGGTATG;

Real-time PCR was performed using the SensiFAST SYBR real time PCR kit (Bioline). Delta CT and melting curves were analyzed. Relative charging levels were expressed relative to the non-oxidized control.

Immunofluorescence

Cells were grown on glass coverslips and rinsed two times with ice-cold PBS before fixation with 4% paraformaldehyd/PBS for 10 min at room temperature (RT). Cells were then rinsed three times with PBS, permeabilized with 0.5% Triton X-100/PBS for 10 min at RT, and washed two times for 5 min with PBS. After blocking with PBG buffer (0.2% fish skin gelatin, 0.5% BSA in PBS) for 1 hr at RT, cells were incubated with a primary antibody against γH2AX (Ser139) (5636-I, Millipore, 1:3,000) diluted in PBG buffer for 2 hours at RT. Cells were then washed three times for 5 min with PBS and incubated with an IgG secondary antibody (Alexa 647 goat anti-mouse IgG, A21235, Thermo Fisher Scientific, 1:500) diluted in PBG buffer for 1 hr at RT. After washing three times for 5 min with PBS, coverslips were mounted onto glass slides using ProLong Gold Antifade Mountant with DAPI (P36931, Thermo Fisher Scientific). Slides were visualized using a Zeiss LSM 980 confocal with Airyscan2 with ZEN 2.6 software at 63X magnification. At least 100 cells were counted per condition.

Cell competition assay

GFP or mCherry labeled MDA-MB-231 and A549 cells were treated with arginine depletion medium supplemented with either cysteine or cystine (C2) for 72 hours, then harvested and recovered in normal medium for 1 hr. Subsequently, cells were counted and seeded at 4:6 ratio in 12-well plates at a concentration of 100,000 cells per ml. Cells were treated with cisplatin at the indicated concentration for 48 hours, then refreshed with a normal cell culture medium. Cell populations were kept in culture for 3 weeks when the percentage of green and red fluorescent cells was determined by FACS analysis on LSR Fortessa (BD).

Cell survival assay

MDA-MB-231 cells were treated with media depleted for either arginine or control tryptophan and supplemented with either cysteine or C2 for 72 hours. Then, cells were recovered for 1 hr in a normal medium (containing C2), subjected to cisplatin treatment for 48 hours, washed and further cultured for 2 weeks. After washing with PBS, cell plates were fixed with 4% formaldehyde and stained with 0.1% crystal violet for 30 min. Before scanning the plates, cells were washed 6 times with water and air dried. The dye of the cells was extracted by 10% acetic acid, and the absorbance was measured on Infinite M Plex (Tecan) reader at 590 nm.

Metabolism measurements

Cells were washed with ice cold PBS and metabolites were extracted in 1 mL lysis buffer containing methanol/acetonitrile/dH2O (2:2:1). 5 mM iodoacetamide (IAA) was added to alkylate the thiol groups of cystine and glutathione. Samples were shaken and centrifuged at 16.000g for 15 minutes at 4 °C to remove cell debris and supernatants were collected for LC-MS analysis.

LC-MS analysis was performed on a Q-Exactive HF mass spectrometer (Thermo Scientific) coupled to a Vanquish autosampler and pump (Thermo Scientific). The MS operated in polarity-switching mode with spray voltages of 4.5 kV and -3.5 kV. Metabolites were separated using a Sequant ZIC-pHILIC column (2.1 x 150 mm, 5 μm, guard column 2.1 x 20 mm, 5 μm; Merck) with elution buffers acetonitrile (A) and eluent B (20 mM (NH4)2CO3, 0.1% NH4OH in ULC/MS grade water (Biosolve)). Gradient ran from 20% eluent B to 60% eluent B in 20 minutes, followed by a wash step at 80% and equilibration at 20%. Flow rate was set at 100 μl/min. Analysis was performed using Tracefinder software (Thermo Scientific). Metabolites were identified and quantified on the basis of exact mass within 5 ppm and further validated by concordance with retention times of standards. Peak intensities were normalized based on the signal of IAA.

Generation of Search Database

UNIPROT (UP000005640) human proteome was downloaded from the UNIPROT server. All arginine amino acids were substituted with every other amino acid and tryptic peptide spanning the substituted amino acid was extracted using a custom script written in PERL. This FASTA library is labeled as "Substitution Library". This substitution library was concatenated to the original UNIPROT library with the addition of the generated substitution peptides such that all wild-type sequences are included. The library was optimized with the addition of reverse decoys contaminants using Philosopher (ref) with the command 'philosopher database –custom <file_name> –contam'

Scanning of Database

OVSCC, LSCC, LUAD, UCEC, PDA, HCC, HNSCC, PDA, and GBM proteomics samples were retrieved from the Proteomics Data Center Commons (PDC) in MZML file format. We analyzed a total of 1686 samples from nine cancer types (tumors (T)=1025; and adjacent normal tissue (ANT)=661), of which OVSCC (Ovarian squamous cell carcinoma PDC000110, T=84, and ANT=22), LSCC (Lung squamous cell carcinoma PDC000234, T=108 and ANT=99), LUAD (Lung adenocarcinoma PDC000153, T=114 and ANT=103), UCEC (endometrial cancer PDC000125 T=100 and ANT=49), PDA (pancreatic adenocarcinoma PDC000270, T=137 and ANT=74), CCRCC (Clear cell renal cell carcinoma PDC000127, T=110 and ANT=84), HCC (hepatic cellular carcinoma PDC000198, T=165 and ANT=165), GBM (Glioblastoma PDC000234, T=100 and ANT=10), and HNSCC (Head and neck squamous cell carcinoma PDC000221, T=105 and ANT=54). The PDC identifiers are listed in the key resource table. The generated substituted library was scanned using Philosopher with the parameters as detailed in File S1 (In short, run Philosopher using the pipeline command, then input the file. Detailed instructions can be found on https://github.com/Nesvilab/philosopher/wiki/Pipeline-mode-for-TMT-analysis). Briefly, MSFragger scans with the following parameters were used; Precursor mass lower: −20 ppm, Precursor mass upper: 20 ppm, precursor mass tolerance: 20 ppm, calibrate mass: True, Deisotoping: True, mass offset: False, isotope error: Standard, digestion: Strictly tryptic (Max. missed cleavage: 2), Variable modifications (For TMT datasets): 15.99490 M 3, 42.01060 [^ 1, 229.162932 n^ 1, 229.162932 S 1, Variable modifications (For iTRAQ datasets): 15.99490 M 3, 42.01060 [^ 1, 144.1021 n^ 1, 144.1021 S 1, Min Length: 7, Max Length: 50, digest mass range: 500:5000 Daltons, Max Charge: 2, remove precursor range: −1.5, 1.5, topN peaks: 300, minimum peaks: 15, precursor range: 1:6, add Cysteine: 57.021464, add Lysine (for ITRAQ datasets): 144.1021, add Lysine (for TMT datasets): 229.162932,among other default parameters. Peptide validation was undertaken using PeptideProphet with the following parameters (accmass: TRUE, decoyprobs: TRUE, expectScore: TRUE, Glycosylation: FALSE, ICAT: FALSE, masswidth: 5, minimum probability after first pass of a peptide: 0.9, minimum number of NTT in a peptide: 2, among other parameters (Supplemental File S1). Next, isobaric quantification was next undertaken separately for TMT samples with the following parameters (bestPSM: TRUE, level: 2, minProb 0.7, ion purity cut-off: 0.5, tolerance: 20 ppm, among other parameters. Thereafter, FDR filtering was implemented to retain only confident peptides with the following parameters (FDR < 0.01,

peptideProbability: 0.7, among other parameters (File S1). Thereafter, TMT-integrator (ref) was used to integrate isobaric quantification with the following parameters (retention time normalization: False, minimum peptide probability on top of FDR filtering (TMT datasets): 0.9, minimum peptide probability on top of FDR filtering (for iTRAQ dataset): 0.5, among other parameters).

Retaining arginine substitutions
Only those arginine substitutions that were sourced from proteins that were identified to be expressed were retained for the downstream analysis. The proteins that are detected in CPTAC analysis, i.e. PDC commons, using CDAP protocol (https://pubmed.ncbi.nlm.nih.gov/26860878/) in relevant datasets, were considered to be expressed.

PEPQUERY validation
The detected arginine substitutions were evaluated for validation with a "peptide-centric" approach using PEPQUERY2. The parameters for PEPQUERY were equalized to the Philosopher runs as follows; (-b dataset_name -db swissprot:human -maxLength 55 -tol 20 -o output_foler -i pep_list.txt)

Characterization of R>C Substitutants
The detected R>C substitutants were checked for overlap with genetic mutations with the analysis performed in the original study [Satpathy et al.[27], A proteogenomic portrait of lung squamous cell carcinoma]. The protein expression profiles were downloaded from the PDC (Proteomic Data Commons) for every cancer type. The codon analysis was undertaken using GENCODE (v19) transcript and translation files with a custom PERL script.

Proteomics – sample preparation and LC-MS/MS
Immunoprecipitation beads were resuspended in 1x S-Trap lysis buffer and heated at 950C for 7 min. in the presence of 20mM DTT. Supernatants were transferred to new 1.5mL tubes, after which proteins were alkylated with 40mM iodoacetamide (30 min. at RT in the dark). Finally, proteins were digested o/n with trypsin (Sigma-Aldrich; enzyme/substrate ratio 1:10) on S-Trap Micro spin columns according to the manufacturer's instructions (ProtiFi, NY, USA). Peptides were eluted, vacuum dried and stored at -80°C until LC-MS/MS analysis. LC-MS/MS was performed by nanoLC-MS/MS on an Orbitrap Exploris 480 mass spectrometer (Thermo Scientific), connected to either an Easy nLC1200 LC system (Thermo Scientific) or an Evosep One LC system (Evosep Biotechnology, Odense, Denmark). Prior to LC separation with the Evosep One, peptides were reconstituted in 0.1% formic acid and 20% of the sample was loaded on Evotip Pure (Evosep) tips. Peptides were then eluted and separated using the pre-programmed "Extended Method" (88 min gradient) on an EV1137 (Evosep) column with an EV1086 (Evosep) emitter. Nanospray was achieved using the Easy-Spray NG Ion Source (Thermo Scientific) operated at 2 kV.

Prior to LC separation with the nLC1200, peptides were reconstituted in 2% formic acid, after which 10% of the sample was directly loaded onto the analytical column (ReproSil-Pur 120 C18-AQ, 2.4μm, 75 μm × 500 mm column, packed in-house in fritted Empty Self Pack NanoLC column tubes with integrated emitter tip (CoAnn Technologies LLC, WA, United States). Peptides were eluted in a 80-minutes gradient containing a 68-min. linear increase from 7% to 26% solvent B (solvent A was 0.1% formic acid/water and solvent B was 0.1% formic acid/80% acetonitrile), followed by washout at 90% solvent B. Nanospray was achieved using the Nanospray FlexTM Ion source (Thermo Scientific) with a liquid junction set-up at 2.0 kV. On the Exploris 480, the data-dependent acquisition was performed as follows. Full scan MS was acquired at resolution 60,000 with MS1 mass range 375-1500 m/z, normalized AGC target and maximum injection time were set to "Auto". Dynamic exclusion was set to 15 sec. (Proxeon runs) or 20 sec (Evosep runs), and MS2 spectra were acquired at 15,000 resolution, with data-dependent mode set to a cycle time of 1 sec. Precursors were HCD-fragmented with a normalized collision energy of 30 when their charge states were 2-6; the MS2 isolation window was 1.2 m/z, the normalized AGC target was set to "standard" and the maximum injection time mode was set to "auto".

Proteome analysis for detecting R>C substitutants in MB-231 cells was performed by 2D-LC-MS/MS as described previously.[20,31,63] All mass spectrometry proteomic data generated in this study have been deposited to the ProteomeXchange Consortium via the PRIDE[64] partner repository with the dataset identifier PXD043612 in the key resources table.

Generation of search database
The search databases were generated, to cover all possibilities of aberrant protein production from the V5 reporter protein. We substituted wild-type arginines (R) for every other amino acid, either altogether or independently. These substitutions were appended to wild-type sequence and a new database was generated.

Screening immunoprecipitation–mass (IP/MS) spectrometry data against the databases
The search was performed using MaxQuant (version 1.6.0.16) Tyanova.[65] Peptide false discovery rate (FDR) threshold was set at 0.01. MaxQuant was run in the headless version and the parameters, database file as well as search folder txt are deposited in the PRIDE database (PXD043612).[66]

Screening whole proteome mass spectrometry data for codon-specific R>C substitutants

A database was generated from the human transcript assembly (GENCODE v19). The transcriptome was translated using custom Python scripts. In-frame Arginine and the codon of origin were identified. The resulting database consisted of the wild-type proteome and R>C substituted tryptic peptides for each arginine codon separately. We included W>F substituted tryptic peptides in the database as a control. The search was performed using FragPipe v20.0, and the parameters for the label-free quantification, as defined in the workflow tab were set and deposited in the PXD043612 database.

Briefly, MSFragger searches with Trypsin as a digestive enzyme allowing up to 2 missed cleavages. Variable modifications are set to Met-oxidation and N-term Acetylation. Cysteine+57 is set as a fixed modification. Post-processing is done by Philosopher with FDR set at 1%. Label-free quantification is done by IonQuant. Further parameters are deposited in the PRIDE database (PXD043612). Output 'peptide.tsv' files from each sample was used for further analysis.

QUANTIFICATION AND STATISTICAL ANALYSIS

Cys-index analysis

Cys-index was determined by normalizing the fluorescent signal of protein-incorporated cysteine divided by the protein level signal from the immunoblot analysis, then normalized to the positive control of KRT8s-Cys-V5 signal of the same experiment.

Cell competition anslysis

At least 3 independent experiments were measured, and the pValues were calculated by one-way ANOVA with Sidak's multiple comparisons test.

Post-scanning analysis for gene-expression correlation and association with genetic mutations

The output file at peptide level: ratio_peptide_None.tsv was used to document the identified peptides from which the substitutant peptides were extracted. The detected peptide intensity score was normalized to the reference channel and the peptide score above 0 (log scale) was considered as a positive peptide for that sample. Density plots, as well as Barplots (Figures 1C, 1F, S1A, and S1B), were plotted for the number of peptide detections. For all substitution inter-tumoral and/or cross-substitutant enrichment analyses, a filter for the maximum number of samples (<25%) was applied to retain peptides with higher specificity in expression and to equalize the distribution of all substitutions (Figures 1A, 1B, 2A, 2B, 5H, and S2). With the assumption of higher false discovery, this was designed to increase biological specificity and control for cross sample and substitutant class noise variance as described previously.[31]

For the non-comparative single substitutant (R>C) based gene expression association study mentioned next, this filter was not applied to optimize signals and increase accountable data as previously described (Figures 5B–5G, S5A, and S5B).

Next, protein expression profiles for each cancer type were downloaded in the format already analyzed by PDC Commons. R- scripts were designed to compute correlation coefficients of R>C numbers in tumors with Protein expression. Gene Ontology analysis was done using ENRICHR for genes with a correlation coefficient > 0.25. For individual gene analysis, the number of substitutions was counted when a gene was lowly expressed (intensity < 0) or highly expressed (intensity > 0).

Stastics and reproducibility

Statistical analyses were performed in GraphPad Prism 9 (GraphPad). Comparisons between more than two groups were performed using by one-way ANOVA with Sidak's multiple comparisons test, showed in Figures 3D, 3F, 4E, 5K, 6D, 6E, and 6G. Statistical significance P-values were labeled accordingly. Throughout the paper, data sets combined at least three independent experiments (Figure 3F KRT8 (R>K) mutation treatments with 2 independent experiments).